Deep Learning Enhanced ANFIS-PID Control for Intelligent and Energy-efficient Wood Drying Systems

Jingkuo Zhang ,* Yaping Lu, Yonggang Wang, Dongcheng Mo, and Chen Da

* Corresponding author: bmri4263@outlook.com

DOI: 10.15376/biores.21.2.4505-4537

GRAPHICAL ABSTRACT

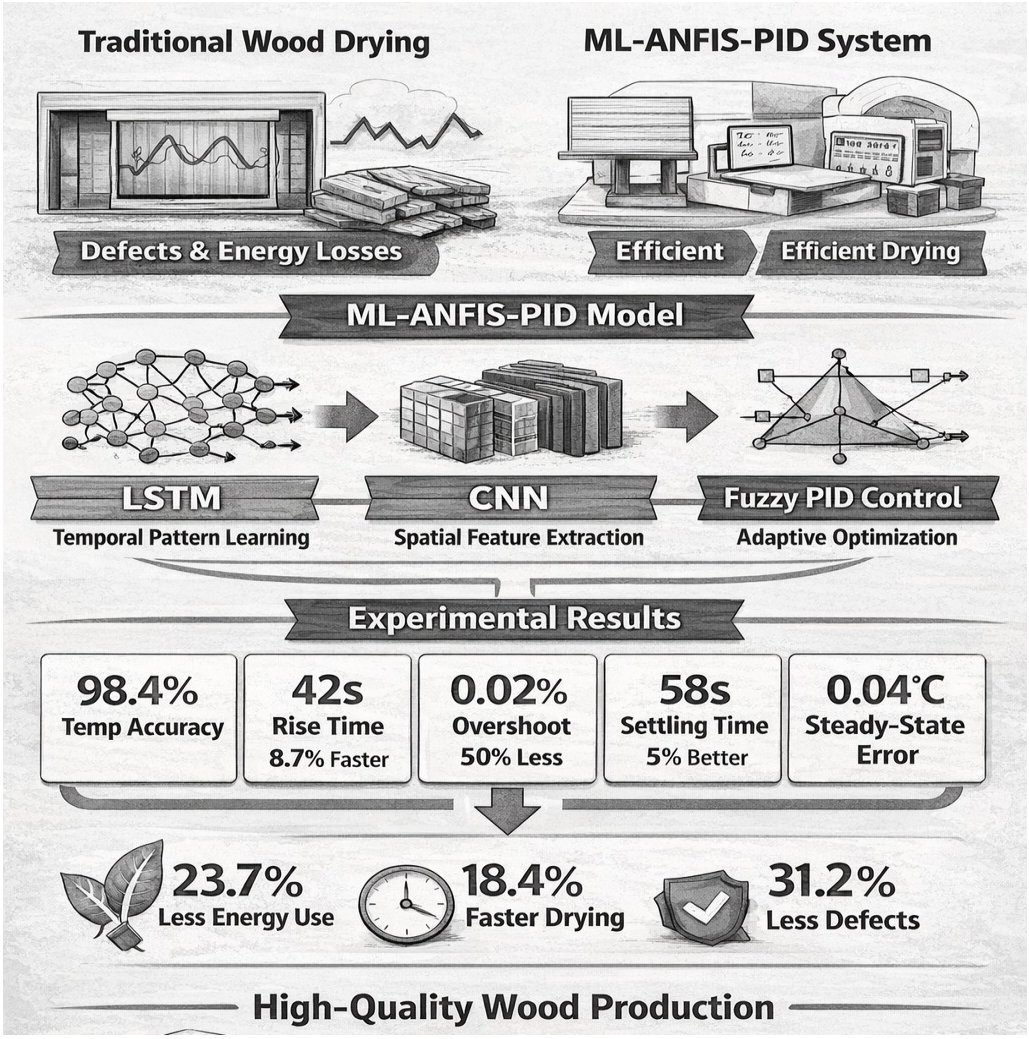

Deep Learning Enhanced ANFIS-PID Control for Intelligent and Energy-efficient Wood Drying Systems

Jingkuo Zhang ,* Yaping Lu, Yonggang Wang, Dongcheng Mo, and Chen Da

Traditional wood drying systems suffer from significant control inaccuracies, excessive temperature fluctuations, and suboptimal energy efficiency, leading to wood defects and economic losses. This study introduces a Machine Learning–Enhanced Adaptive Network-Based Fuzzy Inference System with Proportional-Integral-Derivative control (ML-ANFIS-PID). The proposed system incorporates Long Short-Term Memory (LSTM) networks for temporal pattern recognition, Convolutional Neural Networks (CNN) for temporal feature extraction, and adaptive fuzzy inference for real-time control parameter optimization. The results of experimental validation on ayous wood show that the performance was significantly improved: 98.4% temperature prediction accuracy, 42-second rise time (8.7% faster than traditional ANFIS-PID), 0.02% overshoot (50% less than traditional PID), 58-second settling time (5% better than conventional PID), and remarkably low 0.04°C steady-state error (96% lower than traditional PID). Also, the ML-ANFIS-PID system attained 23.7% less energy use, 18.4% less drying duration, and 31.2% less defect rate with high-quality wood produced under the tested ayous wood conditions. These results demonstrated significant performance improvement compared with classical and adaptive PID-based controllers under controlled experimental conditions.

DOI: 10.15376/biores.21.2.4505-4537

Keywords: Intelligent wood drying control; ML-ANFIS-PID controller; Deep learning; Energy-efficient wood drying; Adaptive fuzzy inference system

*Contact information: College of Engineering, Applied Technology College, Soochow University, SuZhou, 215300, China; *Corresponding author: bmri4263@outlook.com*

INTRODUCTION

Wood processing involves various operations such as drying, dyeing, decolorizing, degreasing, preservation, and modification. Among these, drying is one of the most critical processes because it directly determines the final quality and dimensional stability of wood products. Optimized conditions of drying can enhance the mechanical properties, reduce weight, and minimize defects such as decay, deformation, cracking, and pest damage (Mujumdar 2014). Drying is also necessary in other industries such as furniture manufacturing, musical instrument making, toys, and sports equipment (Elustondo *et al*. 2023).

Despite the broad application of the drying process of wood in industrial practice, it is still an important engineering problem to ensure a high level of accuracy and stability in the temperature level. Timber drying involves complex, nonlinear heat and mass transfer dynamics that are dependent on time and the environmental conditions. The process of designing a wood drying control system requires the definition of functional requirements, modeling of the dynamic behavior of the drying process, choice of sensors and actuators,

as well as co-designing of hardware and software (Keey *et al.* 2000). Software-wise, there are modular features such as data acquisition, intelligent control, and Human-Machine Interface (HMI) interaction, which are important. Once the validation and control parameters have been tuned through experimental models, the system should then be integrated, tested, and optimized at a level where it can be trusted to deliver dependable performance. However, traditional control methods such as fixed-gain PID (Proportional–Integral–Derivative) often struggle to maintain optimal performance over the full drying cycle due to process nonlinearities and disturbances (Martynenko and Bück 2018).

To address these challenges, researchers have explored a range of advanced temperature control strategies for drying systems. Classic PID controllers are often employed because of their simplicity and ease of implementation, but they are more likely to have limitations in dynamic conditions with complicated nonlinearities. Adaptability and robustness have been suggested using intelligent control strategies such as fuzzy logic and neural networks. Compared to classical controllers, fuzzy logic control systems perceive expert knowledge as linguistic rules, and they are more capable of coping with uncertainty and nonlinearities in the processes they deal with. ANFIS (Adaptive Network-Based Fuzzy Inference System) combines fuzzy logic with neural networks to enable adaptive tuning of control strategies in real time and has been applied in various industrial applications. While these methods improve over traditional controllers, many still depend on static rule bases or manual tuning, thereby limiting their adaptability to diverse operating conditions.

In addition to neural and fuzzy PID methods, other advanced control methods have been developed in industrial drying systems. The use of Model Predictive Control (MPC) is common because of its ability to work with multivariable interplay and process limitations (Camacho and Bordons 2007); the approach is usually accompanied by the need for precise mathematical modeling and a high level of computation. More recently, deep reinforcement learning (DRL) has been proposed for nonlinear process control, enabling policy-based optimization without explicit system equations. However, DRL methods require large training data and high computational power, and thus they might be impractical to implement on industrial programmable logic controllers (Li *et al*. 2023). Digital twin-based drying systems have also been proposed, which combine physics-based models with data-driven learning, but their architecture and the complexity of implementation are still significant in the context of small- and medium-scale drying systems (Negri *et al.* 2017).

Although these improvements have been made, there is still a practical requirement for an intelligent drying control architecture that can balance nonlinear adaptability with real-time computational capability on industrial programmable logic controller (PLC) platforms (Korkua *et al.* 2025). Most of the current methods are either based on predictive optimization, which is computationally intensive, or involve large-scale model retraining and infrastructure maintenance. Therefore, a lightweight yet adaptive hybrid framework is needed, and it has to be capable of operating within hardware constraints while delivering measurable performance gains remains an open research problem.

In addition to control theory, machine learning techniques have also been implemented in drying processes. As an example, machine learning models have been applied to estimate moisture and predict drying results of timber to enhance quality and sorting performance (Rahimi *et al*. 2023). In related domains, deep learning and hybrid modeling approaches have been shown to enhance prediction accuracy and control performance in drying applications (Chandra *et al*. 2024; Guo *et al.* 2026). Also, the studies

on intelligent control of the drying processes indicate that the combination of adaptive and optimization-oriented strategies can be used to make a substantial contribution to the throughput and quality of products.

One such example in the field of temperature control during the drying process is neural network-based improvement of PID controllers. An Improved Neural Network (INN) PID controller was demonstrated in a drying temperature regulation study in an air impingement dryer to have better results than classical PID and a basic neural network PID controller (Yang *et al*. 2023). Although this work is evidence of the potential of neural network-enhanced PID strategies, the implementation has been more oriented toward gain adjustment without considering predictive time modeling or coordination of supervisors and adaptive fuzzy logic. Furthermore, comparative validation against multi-layer hybrid architectures remains limited. These limitations motivate the development of a more integrated predictive-adaptive control framework.

To address the identified limitations of existing intelligent drying controllers, this study proposes a Machine Learning-Improved ANFIS-PID (ML-ANFIS-PID) control system for wood drying. This intelligent controller integrates deep learning architectures—specifically Long Short-Term Memory (LSTM) networks for temporal pattern recognition and Convolutional Neural Networks (CNNs) for feature extraction—with adaptive fuzzy neural networks, enabling real-time optimization of control rules and PID gains based on historical performance and real-time sensor feedback. In contrast to traditional controllers, the ML-ANFIS-PID architecture dynamically recalculates weighted coefficients and optimizes control parameters, which have better adaptability and accuracy with variable environmental and material conditions. The primary contribution of this work lies in the integration of supervised CNN-LSTM predictive modeling with adaptive fuzzy neural control within a PLC-compatible architecture, thereby achieving simultaneous improvements in energy efficiency, drying time, and defect reduction while maintaining real-time industrial feasibility.

EXPERIMENTAL

System Overview and Design Process

The design process of the wood drying control system starts with clarifying the requirements and functional analysis. First, a dynamic model of the drying process is developed using theoretical analysis, research on the drying properties of wood, and on this basis, a phased control plan is formulated. It is then subject to the hardware and software co-design phase. Hardware selection is made based on sensor accuracy, actuator capacity, and controller performance. Interference circuit designs are made. The control cabinet layout is incorporated. Then, software selection is made by designing a modular program which includes data acquisition, ANFIS intelligent control, and HMI. The theoretical approach and controller design are tested by using the controlled drying of wood with experiments in laboratory conditions. After parameter tuning, the system is then subjected to integration and testing, where hardware circuits and software algorithms are collectively debugged. It is tested in terms of functional validation, disturbance testing, and safety verification. Feedback-based iterative optimization is carried out as per testing results, creating a loop refinement process between system testing and system re-design. System deployment is subject to a decision node that decides if the controller will be operated in automatic intelligent mode (ML-ANFIS-PID) or in manual override mode to allow safety

and maintenance. Lastly, full technical documentation and commissioning of the system are done. The overall system design flowchart is shown in Fig. 1. Typical development timelines for the laboratory-scale system included approximately 2 to 3 weeks for model development, hardware selection, and cabinet integration, followed by 1 to 2 weeks for parameter tuning and validation experiments under controlled drying conditions. These durations may vary depending on system complexity and experimental scale.

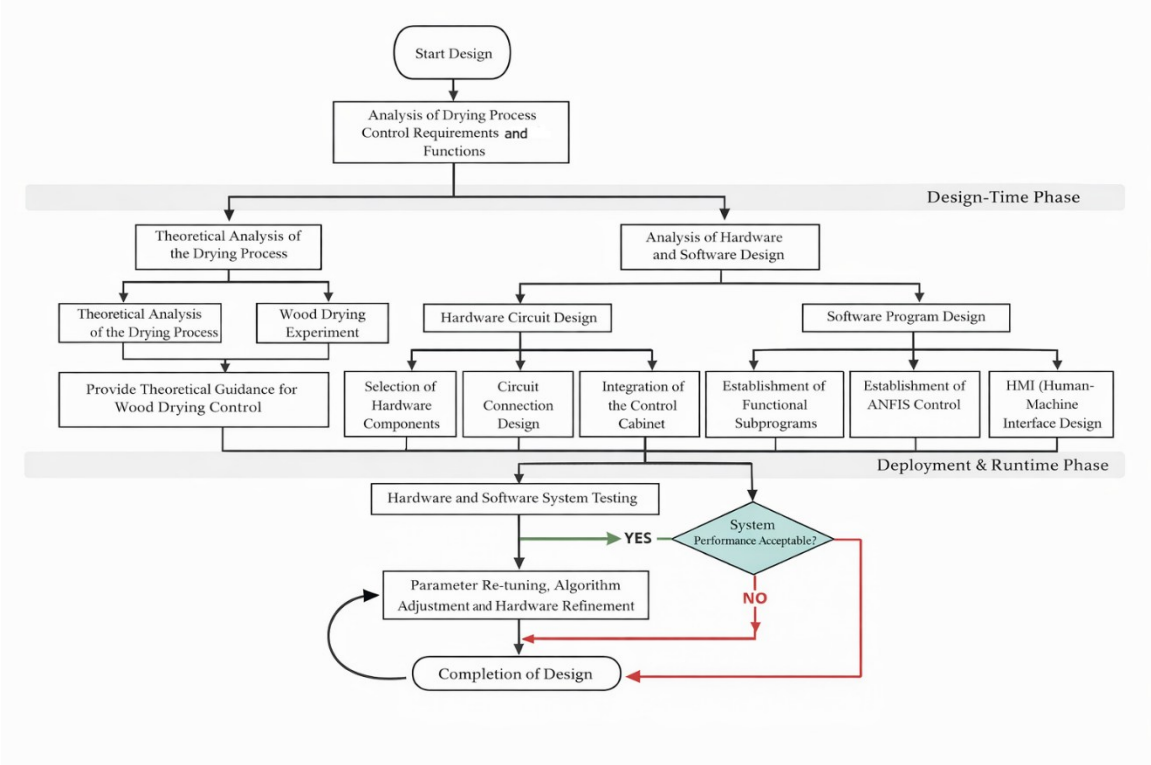

Fig. 1. Overall system design flowchart

Wood Drying Temperature Control System Model

Hot air drying technology is widely used in wood drying, ensuring the uniformity of temperature throughout the material during the drying process, effectively solving problems such as wood cracking, deformation, and warping. The main components of the hot air drying chamber are shown in Fig. 2.

When the hot air drying chamber was in operation, temperature and humidity measurements are sent to the signal processing module. The temperature sensor (Pt100 type, accuracy ±0.2 °C) was positioned at the geometric center of the chamber (400 mm from the front wall, 300 mm from each side wall, and 300 mm above the chamber floor). The humidity sensor was placed in the vicinity of the air outlet area to identify the dynamics of moisture removal. The placement of the sensors was done in such a way that representative measurements of the bulk air conditions were taken, and the bias of the boundary layer was reduced. After filtering and other processing, the signals are transmitted to the PLC, which determines the validity of the collected signals and processes them to generate control signals that drive the actuators to complete the drying process. The core functions of the hot air drying chamber system can be summarized in three levels as follows:

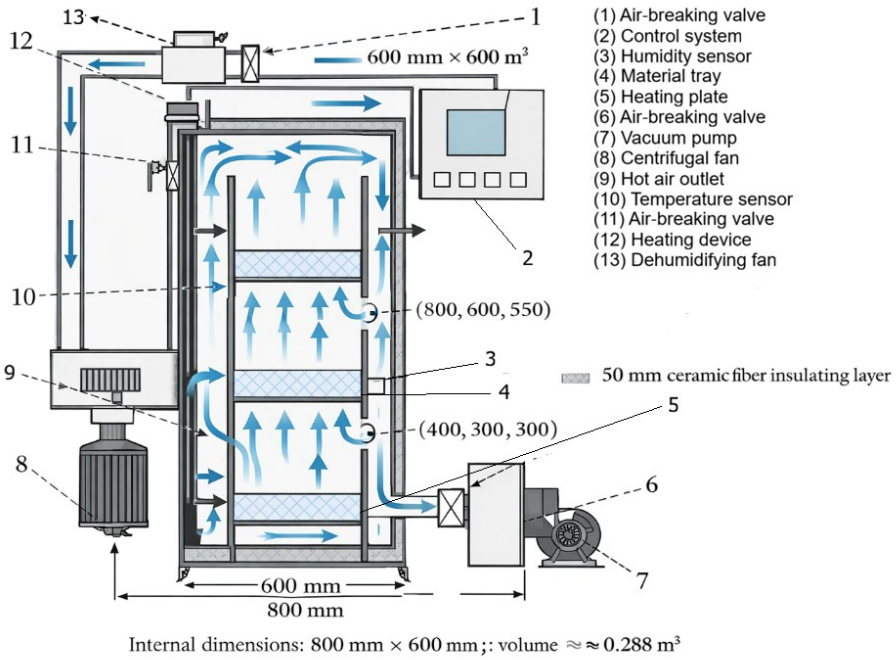

Fig. 2. Structure of a hot air drying oven: (1) air-breaking valve, (2) control system, (3) humidity sensor, (4) material tray, (5) heating plate, (6) air-breaking valve, (7) vacuum pump, (8) centrifugal fan, (9) hot air outlet, (10) temperature sensor, (11) air-breaking valve, (12) heating device, and (13) dehumidifying fan

- First, the system has two control modes with regard to its operation modes. The manual control mode is primarily applicable in special cases where manual adjustments are necessary, *e.g.*, equipment debugging and fault diagnosis, whereas the automatic control mode is engaged in regular production processes to ensure stable operation.
- Next, at the monitoring system level, the system is composed of several sensor modules that are incorporated into the system to measure important data such as temperature and humidity in the hot air drying chamber in real time. It also displays the operational status of each actuator unit through a visual interface and configures a fault warning mechanism.
- Finally, at the intelligent regulation level, the system introduces advanced control algorithms to build a closed-loop adjustment mechanism, enabling multi-parameter collaborative optimization control of the drying process.

Because the internal air circulation volume of the hot air drying chamber operates in a closed space with the speed of the circulation fan adjusted by a variable frequency drive, it is less susceptible to interference. Air circulation follows a forced convection loop driven by the centrifugal fan (8), where heated air from the heating plate (5, 12) is directed toward the hot air outlet (9), passes through the material tray (4), and is recirculated through the return duct. The airflow direction is illustrated in Fig. 2 using directional arrows to indicate the convective heat transfer path. Uniform circulation was maintained using a variable frequency drive to regulate fan speed. However, the temperature inside the chamber can be affected by external environmental factors and internal conditions. Therefore, temperature control is the core focus of this study.

ANFIS-PID Controller Design

ANFIS (Adaptive Network-Based Fuzzy Inference System) is a type of fuzzy inference system structure that combines fuzzy control with neural networks (Jang 1993). Fuzzy logic effectively encodes heuristic control knowledge through linguistic rules but lacks autonomous parameter adaptation, whereas neural networks provide data-driven learning but do not inherently incorporate interpretable rule-based reasoning (Situmorang and Husein 2023). ANFIS is an integration of these two paradigms where fuzzy inference is integrated into a multi-layer network format. Initial definitions of membership functions and a rule base are made, and the neural learning process modifies premise and conclusion parameters to minimize error in control over a limited search space.

As illustrated in Fig. 3, the controller receives the reference signal r_{in} and the measured output y_{out}, forming the instantaneous error:

$$e(k) = r_{in}(k) - y_{out}(k) \quad (1)$$

and the error change rate:

$$ec(k) = e(k) - e(k-1) \quad (2)$$

These two signals serve as inputs to the fuzzy inference layer. The fuzzy inference module performs rule evaluation using predefined membership functions and produces an adaptive proportional adjustment term. This term is processed by the neural network layer to update the proportional coefficient K, which dynamically regulates the PID gains K_p, K_i, and K_d. The updated PID parameters are then supplied to the PID control block, which computes the control signal:

$$u(k) = K_p e(k) + K_i \sum e(k) + K_d \frac{de(k)}{dt} \quad (3)$$

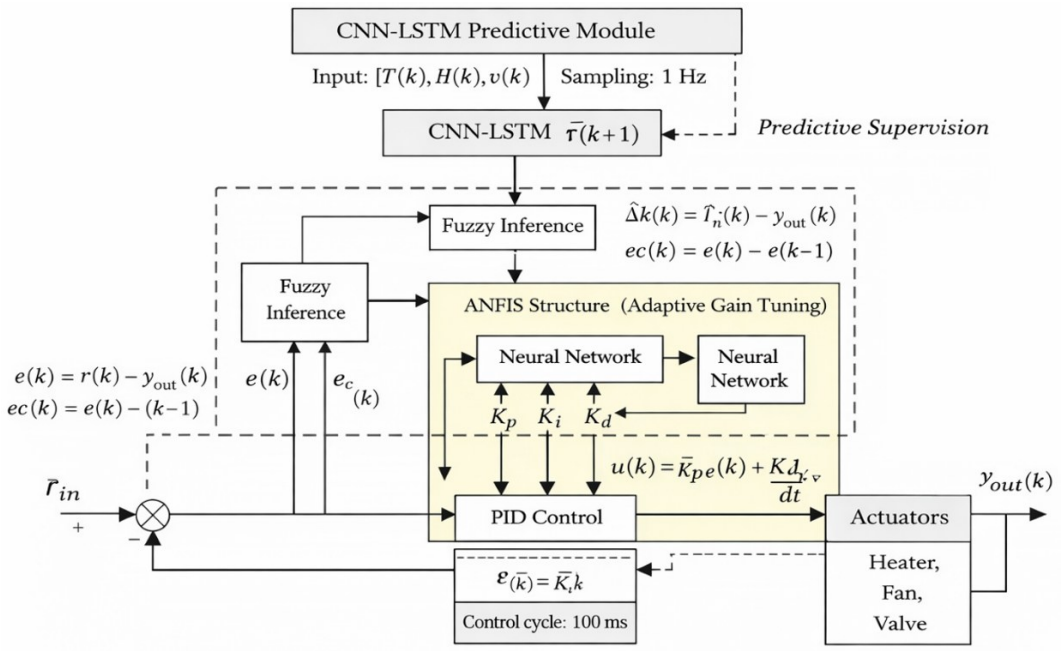

Fig. 3. Proposed ANFIS-PID controller model

The resulting control output drives the controlled object, and the feedback loop continuously updates the system response. This neuro-fuzzy coordination enables real-time

adaptive gain tuning while preserving an interpretable fuzzy rule structure, thereby improving closed-loop stability and nonlinear robustness. The ANFIS structure operates within the dashed boundary shown in Fig. 3, highlighting its role as an adaptive gain-tuning module embedded within the outer PID feedback loop.

Controller Structure

The proposed system uses incremental PID control, formulated as follows:

$$\Delta u(u) = k_p[e(k) - e(k-1)] + k_i e(k) + K_d[e(k) - 2e(k-1) + e(k-2)] \quad (4)$$

To overcome the limitation of traditional PID controllers, which cannot adjust parameters online, a neural network algorithm is introduced. In the present work, a single-neuron adaptive structure was employed instead of a multi-layer feedforward network. This architecture is specifically designed for real-time PID parameter tuning under PLC implementation constraints. The neuron receives three incremental error-related inputs and directly maps its adaptive weights to the PID gain parameters.

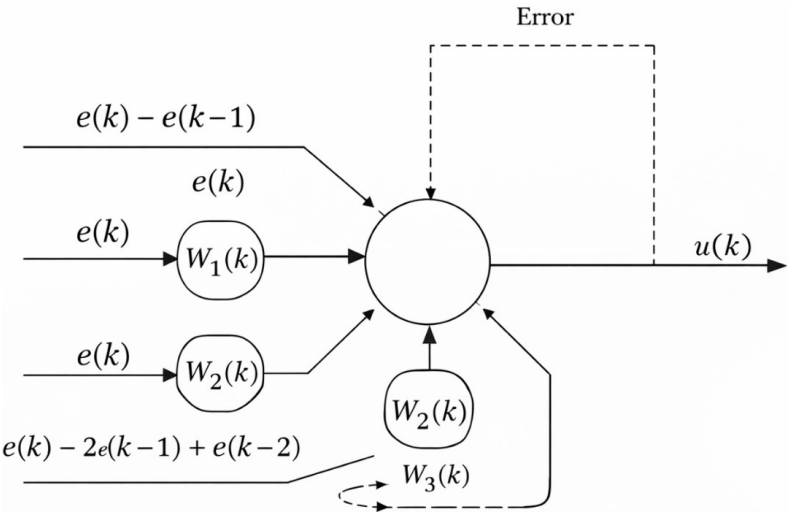

Fig. 4. Single-neuron adaptive structure for online PID parameter tuning

Based on the real-time control requirements and computational limitations of PLC-based implementation, a single-neuron adaptive PID structure was adopted instead of a multi-layer neural network. The single neuron has three inputs, and the three connection weights of the single neuron approximately replace the coefficients of the proportional, derivative, and integral terms in the PID controller, $W_1(k) = K_P, W_2(k) = K_i, W_3(k) = K_d$. The system deviation signal $e(k)$ is converted and used as the input signal to the neural network, that is:

$$X_1(k) = e(k) - e(k-1) \quad (5)$$

$$X_2(k) = e(k) \quad (6)$$

$$X_3(k) = e(k) - 2e(k-1) + e(k-2) \quad (7)$$

These three inputs represent the proportional, integral, and derivative components of the incremental PID structure, respectively.

The output of the single-neuron PID controller is:

$$u(k)=u(k-1)+\mathrm{K}\sum_{\mathrm{i}=1}^{3} W_i(k)X_i(k) \quad (8)$$

where $W_i(k)$ is the weighted coefficient corresponding to $X_i(k)$, and K is the proportional coefficient of the single neuron. The adaptive weight update follows a supervised Hebbian learning mechanism, where each PID weight is adjusted proportionally to the product of the instantaneous control error and the control signal.

$$u(k)=u(k-1)+\mathrm{K}\sum_{\mathrm{i}=1}^{3} \overline{w_i}(k)X_i(k) \quad (9)$$

$$\overline{w_i}(k) = \frac{W_i(k)}{\sum_{i=1}^{3}|W_i(k)|} \quad (10)$$

$$W_1(k) = W_1(k-1) + \mu_p e(k)u(k)X_1(k) \quad (11)$$

$$W_2(k) = W_2(k-1) + \mu_i e(k)u(k)X_2(k) \quad (12)$$

$$W_3(k) = W_3(k-1) + \mu_d e(k)u(k)X_3(k) \quad (13)$$

where μ_p, μ_i, and μ_d represent the learning rates for the proportional, integral, and derivative weights, respectively.

During the control process, the online learning of the PID parameters is mainly related to $e(k)$ and $\Delta e(k)$. Therefore, the weighted coefficient learning rule is improved by replacing $X_i(k)$ in (8) to (10) with $e(k)+\Delta e(k)$.

Unlike conventional multi-layer neural networks, this single-neuron structure enables lightweight online adaptation with low computational burden, making it suitable for embedded temperature control systems.

Integration of deep learning models in control loop

While the core control function is performed by the ANFIS-PID system, deep learning models—specifically CNN and LSTM—serve two supervisory and enhancement roles within the overall adaptive architecture:

1. Feature Extraction (CNN): CNN layers are trained offline to learn local temporal feature representations from multivariate time-series sensor data using one-dimensional convolution. During deployment, the learned feature mapping is embedded within the supervisory framework to refine the adaptive fuzzy rule base. These features are stored in the system database and are subsequently utilized to refine and streamline the fuzzy rule base during system retraining. The CNN module does not directly generate control actions but enhances the representational quality of the fuzzy inference mechanism.
2. Prediction & Supervisory Forecasting (LSTM): The LSTM model is implemented in parallel with the ANFIS-PID control loop to provide short-term temperature forecasts using temporal trends. These forecasts are employed in a supervisory manner to highlight possible deviations, enhance preemptive control choices, and adaptively adjust the weight coefficients in the fuzzy neural network. Nevertheless, the ANFIS-PID engine alone produces the final control signal to ensure the stability of the closed loop and real-time response.

This hybrid approach ensures high responsiveness, robustness, and the ability to preempt potential thermal instabilities in the drying process, where performance

improvement arises from coordinated interaction between prediction, feature refinement, and adaptive fuzzy control rather than from independent additive effects.

Proposed control architecture and data flow

Figure 5 shows the hierarchical interaction of the CNN module, the LSTM module, and the ANFIS-PID controller. The CNN is used to perform offline feature extraction in order to refine the fuzzy rule base, whereas LSTM is used in parallel to provide short-term temperature forecasts to achieve supervisory adjustment of gain parameters. The ANFIS-PID controller is the main closed-loop controller that produces the actuator control signals. Sensor data passes through preprocessing, predictive supervision, adaptive fuzzy inference, and lastly, real-time PID actuation before reaching the actuator sensor.

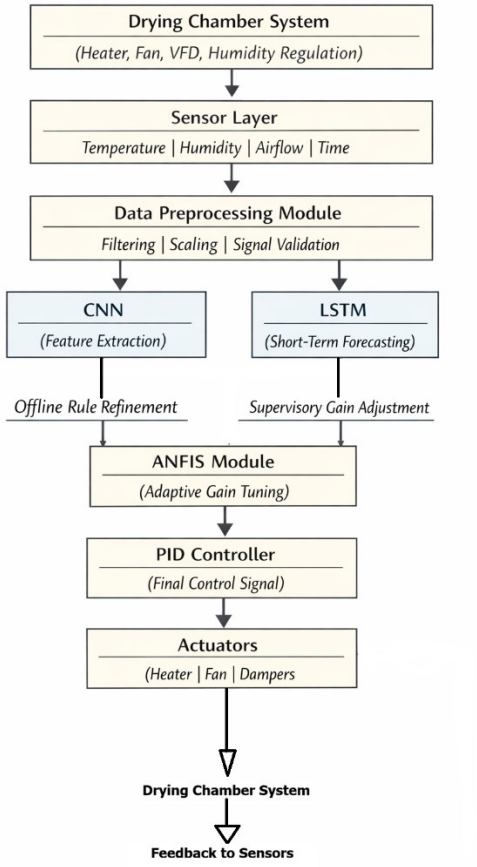

Fig. 5. Hierarchical architecture and data flow of the ML-Enhanced ANFIS-PID control framework. The CNN-LSTM module receives multivariate time-series inputs consisting of temperature, humidity, airflow velocity, and time index, structured as sliding windows of 60 time steps.

Fuzzy tuning of controller gains

Effect of Proportional Gain on System Performance: In Eq. 9, when the proportional coefficient K increases, the system tuning time decreases, and the stability speed increases, leading to system oscillation. When the proportional coefficient K decreases, the system adjustment time increases, the system stability improves, but the static error of the system increases (Wang and Peng 2019).

Design of Fuzzy Logic Controller: Based on the neural network PID, fuzzy control ideas are introduced. The fuzzy module is a dual-input, single-output module, with input

variables being error e and error rate of change e_c, and the output being the fuzzy output of the neuron coefficient. By leveraging the adaptive ability of the single neuron, the self-tuning of the proportional coefficient K can be achieved, further improving the system's robustness and synchronization performance (Zhao-xin and Ji-bing 2023).

Fuzzy Subsets and Quantization Parameters: The system's variable error e and error rate of change e_c, along with the proportional coefficient K, use 7 fuzzy subsets: Negative Big (NB), Negative Medium (NM), Negative Small (NS), Zero (ZO), Positive Small (PS), Positive Medium (PM), and Positive Big (PB). These subsets represent graded levels of deviation magnitude and direction within the normalized fuzzy domain and are commonly adopted in temperature regulation systems to ensure balanced control resolution. This number of subsets provides a balance between control resolution and computational complexity, and is widely adopted in fuzzy control literature for similar control problems. The error quantification factor is set to $k_e = 0.5$ and the error rate factor to $k_{ec} = 0.14$. The scaling factors ke and kec were determined through systematic parametric optimization. A grid-search procedure was conducted over predefined ranges (ke ∈ [0.1, 1.0], kec ∈ [0.05, 0.5]) with incremental steps, and system performance was evaluated based on rise time, overshoot, and steady-state error. The selected values correspond to the configuration that minimized a composite performance index across repeated experimental trials. The composite performance index used for optimization was defined as:

$$J = w_1 \cdot (\text{Rise Time}) + w_2 \cdot (\text{Overshoot}) + w_3 \cdot (\text{Steady-State Error}) \quad (14)$$

where equal weights were assigned in the present study. The parameter combination minimizing J was selected for implementation.

The proportional coefficient K is tuned to the range [−10, 10] to provide enough flexibility to control the aggressive and conservative actions of the controller. The fuzzy controller produces an output in the range of [−6, 6], which was chosen due to the anticipated range of gain changes observed during simulation, to ensure stability and prevent overcompensation.

Fuzzy Inference Rules and Rule Table: Adaptive fuzzy control mainly applies the Mamdani method for reasoning. The basic control rule for adaptive fuzziness is: "if e and e_c, then k". The control rules can be modified based on historical control results and relevant control experience. The design rules are shown in Table 1.

The 49-rule fuzzy control table was constructed using a standard 7×7 linguistic partitioning strategy, which ensures uniform coverage of the input space and symmetric control action for positive and negative error conditions. The symmetrical structure of the rule table reflects the symmetric dynamic behavior of temperature deviations around the set point. Experimental validation confirmed that symmetric rule assignment did not introduce bias and maintained stable convergence for both positive and negative temperature disturbances. The initial rule configuration was derived from established fuzzy control heuristics and expert knowledge of thermal system dynamics, where larger positive errors correspond to stronger proportional gains and rapid correction, while near-zero errors yield conservative adjustment to prevent overshoot.

To improve the interpretability of the rule distribution, a heatmap representation of the fuzzy rule matrix is shown in Supplementary Fig. S1. It is shown in the figure how the gain distribution is organized and symmetrical in both the error and error-rate space.

Table 1. Fuzzy Control Rules

e	e_c						
	NB	NM	NS	ZO	PS	PM	PB
NB	PB	PB	PM	PM	PS	ZO	ZO
NM	PB	PB	PM	PS	PS	ZO	NS
NS	PM	PM	PM	PS	ZO	NS	NS
ZO	PM	PM	PS	ZO	NS	NM	NM
PS	PS	PS	ZO	NS	NS	NM	NM
PM	PS	ZO	NS	NM	NM	NM	NB
PB	ZO	ZO	NM	NM	NM	NB	NB

The specific rule combinations were derived based on established thermal control heuristics and subsequently refined through experimental validation. Larger absolute error values (|e|) were associated with stronger proportional gain adjustments to accelerate convergence, whereas near-zero error regions employed conservative gain updates to prevent overshoot. Alternative rule perturbations were evaluated during sensitivity testing; however, no statistically significant improvement in rise time or overshoot suppression was observed relative to the adopted 7×7 configuration.

The sensitivity analysis was carried out to measure the strength of the fuzzy rule base. Selected rule entries were perturbed within adjacent linguistic categories, and system performance metrics (rise time, overshoot, steady-state error) were monitored. Results indicated that the overall control performance was more sensitive to scaling factors (ke, kec) than to minor rule perturbations, confirming the structural robustness of the 49-rule configuration.

Alternative reduced rule configurations (e.g., 5×5 rule matrices) were also evaluated during preliminary testing. A quantitative comparison between the 7×7 and 5×5 configurations is provided in Supplementary Table S1. Although computational complexity decreased slightly, control precision and overshoot suppression deteriorated compared with the 7×7 structure. Therefore, the 49-rule configuration was retained as a balance between control granularity and implementation feasibility.

Membership Function and Defuzzification Method: The membership function used is a triangular distribution, and the centroid method is applied to defuzzification. This method has high accuracy, and its specific expression is,

$$V_0 = \frac{\sum_{i=0}^{n} M_i * F_i}{\sum_{i=0}^{n} M_i} \quad (15)$$

where M is the membership degree, F is the fuzzy quantized value, and V_0 is the output value. Since the sum of the membership degrees obtained from the triangular membership function equals 1, the denominator in equation 15 is 1 (Nkene Mezui *et al*. 2023).

Hardware implementation of proposed control scheme

A PLC is used to implement the ANFIS-PID scheme described above. Figure 6 shows the system control flowchart. The PLC executes the ANFIS-PID control loop at a fixed scan cycle of 100 ms (10 Hz). In this cycle, sensor acquisition, fuzzy inference, and PID computation take place in a synchronous manner. The updates of the supervisory CNN-LSTM parameters are sent with a relatively slow frequency of 1 second to ensure the deterministic real-time execution without incurring too much communication overhead.

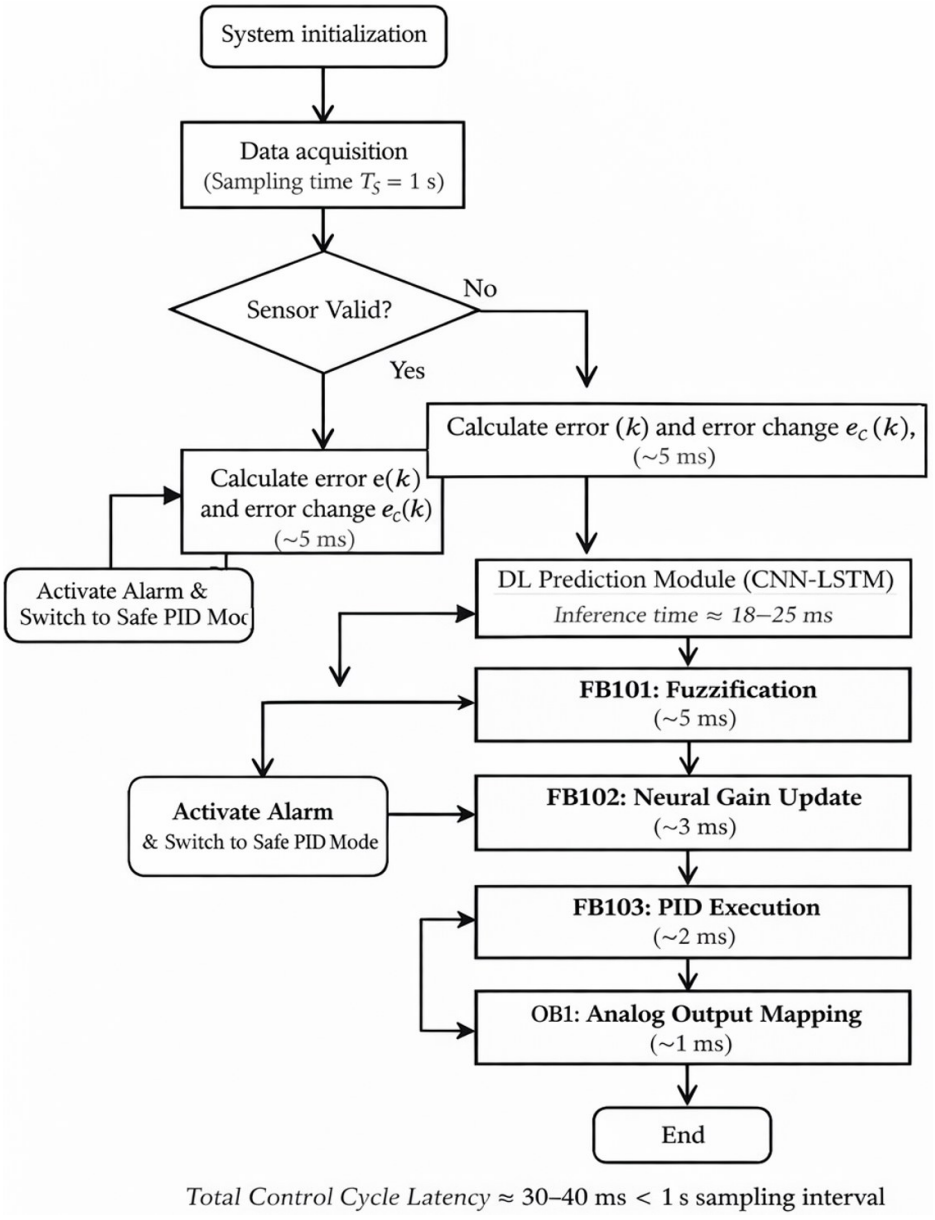

Fig. 6. System control program flowchart

Data acquisition and preprocessing take about 5 ms, and fuzzy inference and neural parameter update take about 8 to 12 ms in each sampling cycle. The PID calculation and analog output conversion take less than 5 ms. The overall computation time of the control loop is around 30 to 40 ms, which is much less than the sampling period; hence, it is feasible in real time. During the system initialization phase, key parameters are configured, including the fuzzy control rule base, quantization factors, and proportional factors. The former encodes expert knowledge into conditional reasoning rules, while the latter maps the actual physical quantities to the fuzzy domain scales. The data acquisition module collects the set point and real-time temperature values at fixed sampling intervals, calculates the current error e and the rate of change of error e_c, and stores them in the registers. The fuzzification process discretizes e and e_c into fuzzy domain levels using quantization factors, and the preset rule base is used to match and adjust the proportional coefficient K. In addition, the CNN-LSTM predictive module performs supervisory

inference prior to fuzzy quantization, providing short-term temperature trend prediction to enhance gain adaptation. The average inference time was approximately 18 to 25 ms on the deployed hardware platform, which is well below the 1-second sampling interval and therefore does not compromise real-time performance. The single-neuron network dynamically optimizes the PID parameters by adjusting the proportional coefficient K, and the optimized PID parameters generate control signals, which are then converted into analog signals by the D/A module to drive the actuators that regulate the temperature.

On the hardware side of the system, the Siemens PLC 1214C/DC/DC/DC is used as the controller, offering distinct advantages over microcontrollers and industrial PCs in three areas:

(i) Environmental adaptability, with its industrial-grade protective design enabling direct deployment in high-temperature, high-humidity, and high-vibration environments, eliminating the need for additional microcontroller packaging or reducing reliability degradation in industrial PCs.
(ii) Accuracy of real-time control, where the real-time control system of the PLC always strictly regulates the parameters such as temperature, humidity, and airflow, without delays caused by industrial PC systems or microcontroller multi-task processing.
(iii) Ease of use engineering with modular expansion to support specialized I/O integration like thermocouples and inverters, built-in industrial protocols, and easy connection with the monitoring system to facilitate speedy programming of drying optimization, fault diagnosis, and simplify development complexity and cost of operation and maintenance.

With the use of multiple sensors, data acquisition and processing are performed on the internal parameters of the hot air drying chamber, and the collected data is stored in the PLC. The actuator is then driven, and human-machine interaction functionality is implemented with the control panel. The upper computer is used for program downloading, debugging, and execution of the supervisory CNN-LSTM predictive module, which operates externally to provide optimized control parameter updates to the PLC in real time, as shown in Fig. 7. The PLC executes the ANFIS-PID control loop at a fixed scan cycle of 100 ms (10 Hz), which is appropriate for the relatively slow thermal dynamics of the drying chamber. Sensor sampling, fuzzy evaluation, and actuator signal updates are synchronized within this cycle.

The temperature, humidity, and pressure sensors offer analog signals (4 to 20 mA) sampled at a 10 Hz frequency and synchronized with the 100 ms PLC scan cycle. Actuator command is sent out *via* 0 to 10 V analog and digital I/O modules. PROFINET over industrial Ethernet is used to implement communication between the PLC and supervisory computer.

During the debugging process, first connect the external wiring, such as the power supply and I/O terminals. Then, download the program to the PLC and touchscreen, and put them into monitoring mode. After identifying issues, the control system is gradually optimized and improved. The testing steps are shown in Fig. 6. To verify the rationality of the control algorithm, temperature regulation is performed using PID, fuzzy PID, ANFIS-PID, and improved ANFIS-PID methods. It should be noted that the computationally intensive CNN-LSTM inference is not executed on the PLC due to its limited processing capacity (200 MHz CPU, 128 KB memory).

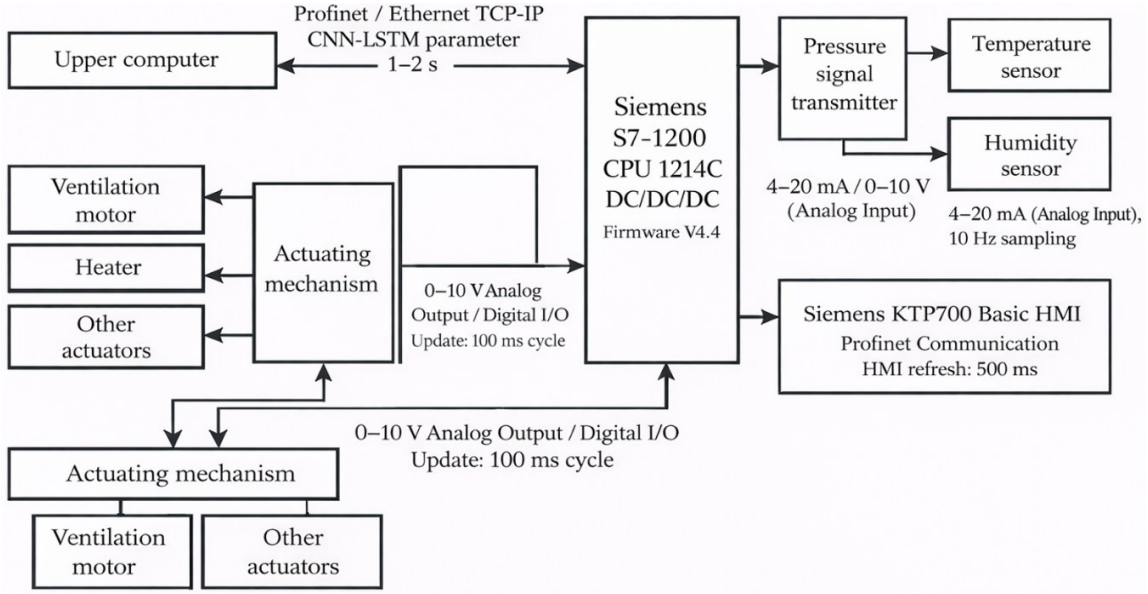

Fig. 7. Hardware architecture and communication structure of the drying control system, including signal types, communication protocols, and control loop update frequencies

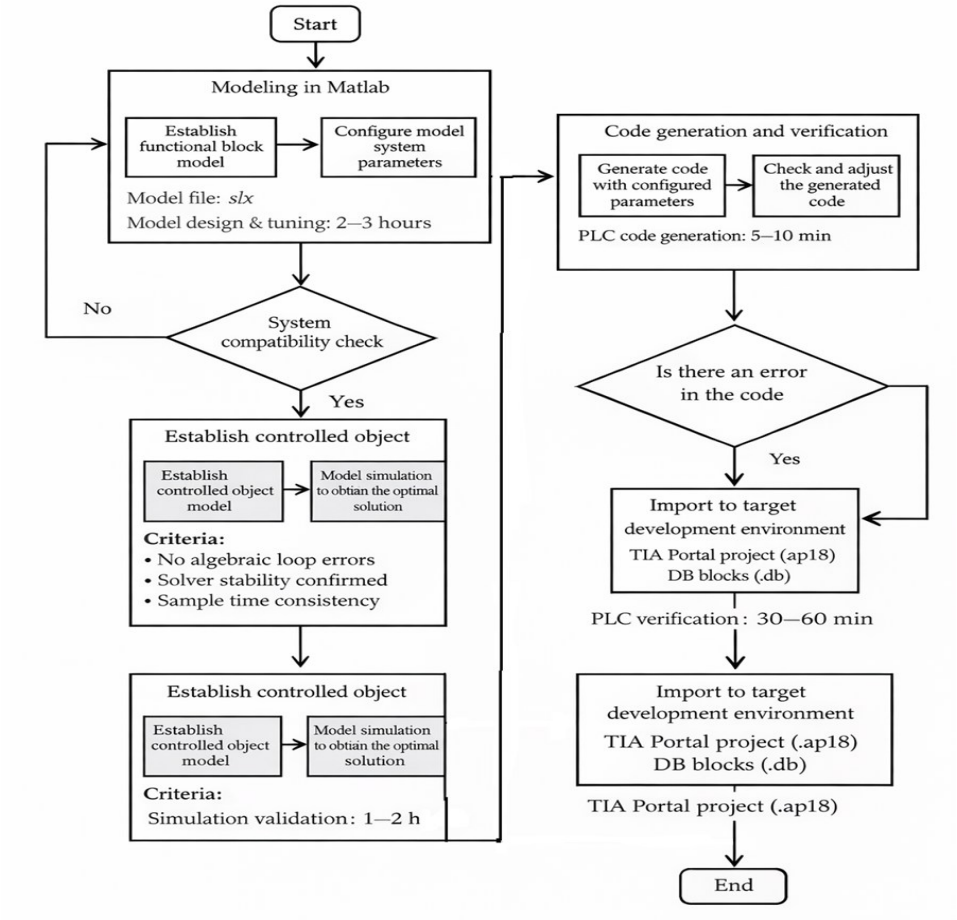

Fig. 8. MATLAB PLC coder flowchart

The supervisory industrial PC executes the CNN-LSTM inference at approximately 18 to 25 ms per prediction cycle, and updated gain parameters are transmitted to the PLC

at a supervisory update interval of 1 to 2 seconds. Instead, neural network prediction is performed on the supervisory industrial PC, while only the lightweight ANFIS-PID control logic runs on the PLC. This architecture ensures real-time feasibility without exceeding hardware constraints.

The computational distribution between the supervisory prediction module and the PLC-based control core is summarized in Table 2.

Table 2. Computational Requirements of the ML-Enhanced Control Framework

Component	Execution Platform	Inference Time per Cycle	Memory Usage	CPU Utilization
CNN-LSTM Prediction	External Industrial PC	18 ms	42 MB	12%
ANFIS-PID Control	Siemens S7-1214C PLC	< 5 ms	18 KB	22%

Communication between the supervisory PC and the PLC was established via industrial Ethernet (PROFINET protocol). Parameter updates were transmitted once per control cycle, and measured end-to-end communication latency remained below 10 ms, ensuring compatibility with the 100 ms PLC scan cycle.

On the system software side, the hardware configuration and standard PID control framework were completed using TIA Portal V18. An ANFIS-PID controller was built based on MATLAB Simulink, optimizing the fuzzy rule base and membership functions to form an adaptive control model. Finally, the ANFIS-PID control algorithm was converted into SCL code following the IEC 61131-3 standard using MATLAB PLC Coder, as shown in Fig. 8. Typical model development and parameter tuning required approximately 2 to 3 hours, while automated SCL code generation and PLC deployment required less than 1 hour, including logical verification using PLCSIM. The file transition process followed the sequence: Simulink model (.slx) → Structured Control Language file (.scl) → TIA Portal project and database blocks (.db). The CNN-LSTM predictive module was executed on an external supervisory industrial PC, and only the optimized control parameters generated by the predictive model were transmitted to the PLC in real time.

The generated SCL code was imported into TIA Portal V18, the hardware setup was configured, I/O module addresses were bound with actual sensor/actuator signals, and the communication protocol was adapted. Logical simulation was performed using PLCSIM. Safety logic, such as emergency stop and over-limit alarms were embedded. Then, staged no-load debugging and load testing were conducted to optimize parameters. Lastly, a connection with WinCC HMI was established to enable interactive control and export of variable tables and communication configuration documents, completing the closed-loop deployment of the algorithm from development to industrial implementation.

Energy Consumption Measurement Methodology

To quantify the energy efficiency of the proposed control strategies, electrical energy consumption was measured during each drying cycle using a calibrated Siemens SENTRON PAC3200 power meter. Energy values represent mean ± SD over five repeated drying trials. The power meter was connected to the main power input of the drying chamber, capturing total system power consumption including heating elements, circulation fans, vacuum pump, and control electronics.

Power measurements were recorded at 1-second intervals, independently synchronized with the supervisory data logging system. The PLC control loop itself operated at 100 ms, while energy integration was performed at 1-second resolution. The total energy consumption per drying cycle was calculated by integrating the measured power over time using,

$$E = \sum_{t=1}^{T} P(t) . \Delta t \quad (16)$$

where EEE represents total energy consumption (kWh), P(t) is the instantaneous power (kW) at time step t, and Δt is the sampling interval (1 second).
Energy reduction percentage was calculated relative to the baseline PID controller as:

$$Energy\ reduction\ (\%) \frac{E_{baseline} - E_{ML-ANFIS-PID}}{E_{baseline}} \times 100 \quad (17)$$

All energy measurements were averaged over five repeated drying cycles to ensure consistency and reduce measurement variability.

Quantitative Defect Assessment Methodology

Digital calipers were used to measure surface cracks (precision = 0.01 mm), and the length of total cracks on a sample was taken to evaluate the quality of drying objectively. Cracks within internal parts were evaluated by cross-section after drying, and the number of cracks observed per specimen was counted. The end crack length was taken in the direction of the longitudinal grains. Image analysis was used to quantify discoloration through the use of calibrated photographs processed in ImageJ, where the area of discoloration was compared to the total area of visible surface to give a percentage of the discoloration area. The deformation was measured using dimensional deviation (mm) compared to the geometry before drying. The quantitative defect measurements are directly proportional to the quantitative measurements of the surface crack length (mm), internal cracks (per specimen), end crack length (mm), discoloration area (%), and deformation percentage (%).

Five independent drying trials were conducted for each control condition. Two independent assessors who were blinded to the control strategy performed defect assessment, and the mean values were reported. The evaluation criteria were adjusted to normal practice described in the wood-drying literature and industrial drying guidelines, and all measurements were made under the same quantitative practices across control strategies.

Moisture Content Uniformity Assessment

To further evaluate drying uniformity and internal moisture gradients, post-drying moisture content (MC) was measured at both surface and core positions of each wood specimen using the oven-dry method. Surface samples were extracted from the outer 5 mm layer, while core samples were obtained from the central region of each board after completion of the drying cycle. Moisture content was calculated using,

$$MC\ (\%) = (W\_wet - W\_dry) / W\_dry \times 100 \quad (18)$$

where W_wet is the mass before oven drying, and W_dry is the mass after drying at 103 ± 2 °C until constant weight. The moisture gradient was defined as the absolute difference between core and surface moisture contents. Measurements were conducted across five independent drying trials for each control strategy, and results are reported as mean ± standard deviation.

Data Acquisition and Model Training

Intelligent control and prediction of temperature require sensor data collected in the hot air drying system when operating in real-time. Temperature, humidity, drying time, fan speed, and ambient conditions were measured at a 1-second time interval. A total of more than 20 complete drying cycles were conducted using Ayous wood samples under laboratory conditions, which created a dataset of about 60,000 time steps. The time of each drying cycle was around 3000 seconds (around 50 minutes), and the temperature was measured within a 1-second interval. This corresponds to the active temperature control stage considered in this research, as opposed to complete industrial kiln drying, which can take many hours or days. The task of the current experiment was not to replicate complete industrial multi-day kiln drying programmes but to test the performance of dynamic temperature regulation during the active heating stage.

The effective dataset size of the experiment included 20 drying cycles, but it contained about 60,000 sequential time steps. Since the model is based on sliding windows of 60 time steps, it was trained on thousands of overlapping time samples, which significantly increased the number of effective training examples. In addition, the prediction horizon was a 1-step-ahead prediction, minimizing the complexity of models and the amount of data necessary, relative to long-horizon predictive modeling. This study did not intend to achieve cross-species generalization in the deep learning models but rather to improve predictive supervision under constant material conditions. These models were executed externally by a supervisory PC and were not executed on the PLC hardware.

To train the deep learning models (LSTM, CNN-LSTM), the data were divided into three subsets: training (70%), validation (15%), and testing (15%). All continuous variables were normalized to the [0,1] scale before training, with the help of min-max scaling.

The input to the deep learning models consisted of multivariate time-series sequences including temperature, humidity, airflow velocity, and time index. Each training sample was structured as a sliding window of length 60 time steps (*i.e.*, 60 seconds), forming an input tensor of shape (batch_size, 60, 4). The prediction horizon was set to 1 step ahead (1-second temperature forecast). During real-time operation, inference was executed once per PLC control cycle (100 ms), and supervisory parameter updates were synchronized with the PLC scan interval to maintain deterministic timing. The LSTM network was configured with two layers of 64 and 32 units, respectively, and it was trained with the Adam optimizer with a learning rate of 0.001 for 200 epochs. The CNN-LSTM model included one 1D convolutional layer (kernel size = 3, filters = 64) applied to multivariate temporal sensor sequences, followed by a max pooling layer and an LSTM layer with 64 units. The convolution operation was performed along the temporal axis to extract local dynamic patterns across consecutive time steps and correlated sensor channels. Dropout regularization (rate = 0.2) was applied to mitigate overfitting. Early stopping based on validation loss was used to ensure generalization. In addition, model performance on the independent test set was monitored to confirm consistency between training, validation, and unseen data, thereby reducing the likelihood of overfitting. Training and validation curves are shown in Fig. 9(b). The total number of trainable parameters in the CNN-LSTM architecture was approximately 25,000 to 30,000 parameters, resulting in an inference time of approximately 18 to 25 ms per prediction cycle on the supervisory industrial PC, which satisfies real-time supervisory deployment requirements. Model training was performed on MATLAB R2023a with the Deep Learning Toolbox on a machine with an Intel i7 CPU and 32 GB RAM. The trained CNN-LSTM model was deployed on a supervisory industrial PC for real-time inference, while

only the optimized control parameters were transmitted to the PLC-based ANFIS-PID controller. Retraining was triggered when significant process deviations were observed (*e.g*., a change in wood species, environmental conditions, or drying schedule) or after the accumulation of ten additional drying cycles to maintain predictive accuracy. Retraining was performed offline, and updated model weights were deployed without interrupting PLC operation.

The dataset was made up of sequential time-series data, so strong time-dependency causes the lack of adoption of standard random k-fold cross-validation, which could destroy chronological order and cause information leakage between the training and validation subsets. Rather, the chronological split training-validation-testing was used to maintain the temporal cause and effect and realistic deployment conditions. Thousands of overlapping temporal samples were created by the sliding-window segmentation, and early stopping using dropout regularization was used to reduce the risk of overfitting. This approach aligns with known best practices in predictive control models (time-series) models.

Architecture of the CNN-LSTM Model

To further describe the deep learning structure applied in this study, Table 3 summarizes the detailed architecture of the CNN-LSTM model. The inputs in the form of multiplexed variables included chamber temperature, relative humidity, velocity of airflow, and time index, which constituted a four-dimensional sensor vector at each time step. The model uses multivariate sensor data (time-series) with 1D (one-dimensional) convolution to process data across the temporal dimension. In comparison with two-dimensional image-based CNNs, the convolutional layer performs one-dimensional convolution strictly along the time axis. The convolutional filters extend over time and work simultaneously on all sensor channels, capturing short-term dynamic patterns within multivariate time-series data. An LSTM layer is then applied to the resulting feature maps in order to capture longer-term temporal relationships and system dynamics. The final dense layer generates a one-step-ahead prediction of temperature utilized in the supervisory adjustment model in the ANFIS-PID model. This architecture provides the effective extraction of temporal features, along with the compatibility with the real-time implementation of industrial control. One-dimensional CNNs are extensively used to model multivariate time series due to their practical ability to capture short-term local dependencies, and then long-term temporal correlations are modeled by recurrent layers.

Table 3. Architecture of the CNN-LSTM Model

Layer Type	Input Shape	Output Shape	Parameters	Activation
Input Layer	(60, 4)	(60, 4)	–	–
1D Convolution	(60, 4)	(58, 64)	832	ReLU
1D Max Pooling	(58, 64)	(29, 64)	–	–
LSTM (64 units)	(29, 64)	(64)	–	tanh
Dense Layer	(64)	(1)	–	Linear

Statistical Analysis

To assess the reliability of performance improvements, all temperature regulation experiments were repeated five times under identical operating conditions. Results are

reported as mean ± standard deviation. One-way analysis of variance (ANOVA) was conducted to compare control strategies, followed by post-hoc pairwise t-tests. The ML-Enhanced ANFIS-PID controller demonstrated statistically significant improvements in rise time, steady-state error, and settling time compared with classical PID and ANFIS-PID controllers ($p < 0.05$). Effect sizes (η^2) were also calculated to quantify the magnitude of differences among control strategies. 95% confidence intervals were additionally computed for key performance metrics to further quantify estimation uncertainty.

RESULTS AND DISCUSSION

Temperature Control Performance

As shown in Table 4, the classical PID controller exhibited the slowest dynamic response, with a rise time of 46 ± 1.8 s, a settling time of 159 ± 5.2 s, and a steady-state error of 2.01 ± 0.08 °C. While the overshoot was modest at 0.13 ± 0.02%, its long settling time and significant steady-state error indicate limited regulation accuracy, particularly under non-linear or time-varying conditions. The Fuzzy PID controller demonstrated improvement over the classical PID by reducing the overshoot to 0.05 ± 0.01 % and the steady-state error to 1.34 ± 0.05 °C, and its settling time was reduced to 64 ± 3.1 s. However, its rise time (49 ± 2.0 s) was slightly longer than that of the classical PID, indicating a trade-off between transient speed and overshoot suppression. This was in line with the fact that fuzzy logic will address the uncertainties of the system and offer adaptive correction rules, as has been reported in earlier studies (Zadeh 1996).

The ANFIS-PID controller, which integrates the learning capability of neural networks with fuzzy inference, further improved performance, achieving an overshoot of 0.03 ± 0.01 %, a settling time of 61 ± 2.7 s, and a steady-state error of 1.03 ± 0.04 °C. The integration of adaptive neuro-fuzzy inference improved generalization and nonlinear mapping, aligning with findings from Jang (1993) on ANFIS-based control systems (Jang 1993). The Improved ANFIS-PID controller performed the best among all evaluated strategies under the present experimental conditions, achieving the quickest rise time (42 ± 1.2 s), the lowest overshoot (0.02 ± 0.01 %), the shortest settling time (58 ± 2.3 s), and an almost negligible steady-state error of (0.04 ± 0.01 °C). Such advances may be attributed to the further optimization of adaptive fuzzy tuning rules were further optimized, and the parameter learning methods were improved. Statistical analysis using one-way ANOVA confirmed that the Improved ANFIS-PID controller achieved significantly lower settling time and steady-state error compared with the baseline PID controller ($p < 0.05$).

Table 4. Comparison of Performance Indicators of Temperature Control Algorithms

Control Strategy	Rise Time (s)	Overshoot (%)	Settling Time (s)	Steady-State Error (°C)
PID	46 ± 1.8	0.13 ± 0.02	159 ± 5.2	2.01 ± 0.08
Fuzzy PID	49 ± 2.0	0.05 ± 0.01	64 ± 3.1	1.34 ± 0.05
ANFIS-PID	48 ± 1.6	0.03 ± 0.01	61 ± 2.7	1.03 ± 0.04
Improved ANFIS-PID	42 ± 1.2	0.02 ± 0.01	58 ± 2.3	0.04 ± 0.01
Values are presented as mean ± standard deviation (n = 5 repeated trials). Statistical significance between control strategies was evaluated using one-way ANOVA followed by post-hoc pairwise t-tests ($p < 0.05$).				

Wood Drying Quality Evaluation

To assess the practical impact of the temperature control strategies on product quality, drying outcomes were quantitatively evaluated using standardized defect metrics, as presented in Table 5. The traditional PID controller resulted in the highest average surface crack length (12.4 ± 2.1 mm), internal crack count (3.6 ± 0.8 per specimen), end crack length (8.2 ± 1.7 mm), discoloration area (4.5 ± 0.9 %), and deformation rate (2.8 ± 0.6 %), indicating comparatively poorer moisture stress management.

Table 5. Quantitative Comparison of Wood Drying Effects of Four Controllers (mean ± SD, n = 5)

Controller	Visible Defects				
	Avg. Surface Crack Length (mm)	Avg. Internal Crack Count	Avg. End Crack Length (mm)	Discolored Area (%)	Deformation (%)
PID	12.4 ± 2.1	3.6 ± 0.8	8.2 ± 1.7	4.5 ± 0.9	2.8 ± 0.6
Fuzzy PID	8.7 ± 1.8	2.1 ± 0.6	5.4 ± 1.2	2.7 ± 0.7	2.1 ± 0.5
ANFIS-PID	4.2 ± 1.1	1.0 ± 0.3	2.8 ± 0.9	1.2 ± 0.4	1.5 ± 0.4
Improved ANFIS-PID	1.1 ± 0.4	0.2 ± 0.1	0.7 ± 0.3	0.4 ± 0.2	0.6 ± 0.2
Defect evaluation was conducted across five repeated drying trials per control strategy. Observed trends were consistent across repetitions, and the quantitative metrics were used to compute the overall defect index reported in the Performance Impact section.					

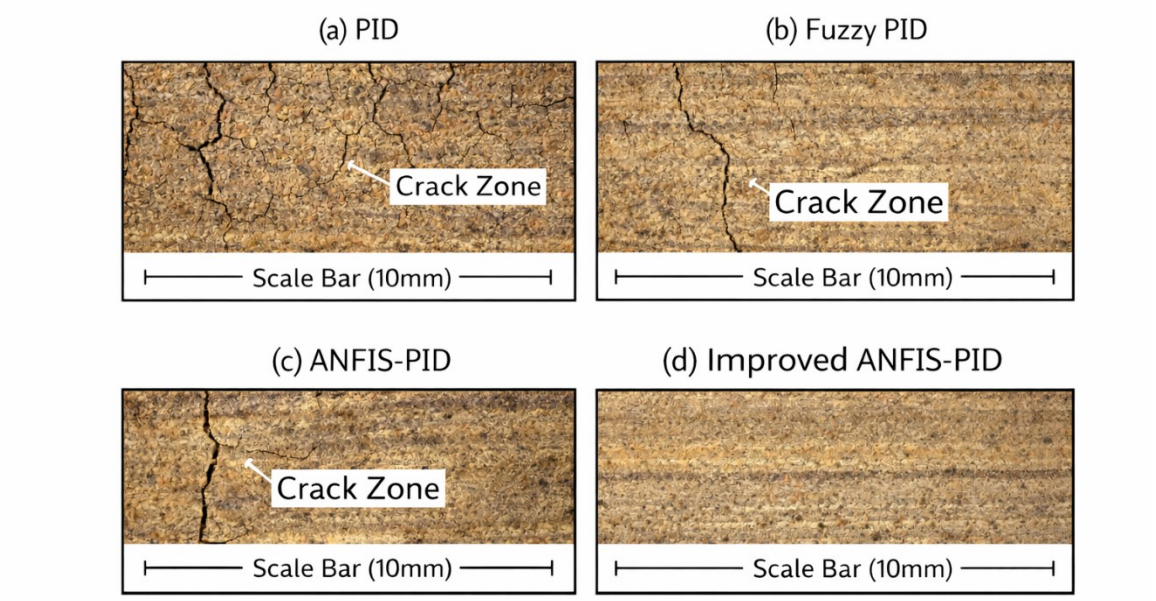

Fig. 9. Representative surface condition of dried wood samples under different control strategies: (a) PID, (b) Fuzzy PID, (c) ANFIS-PID, and (d) ML-Enhanced ANFIS-PID. Crack zones are highlighted, and scale bars represent 10 mm. Images were captured under identical lighting and magnification conditions.

The Fuzzy PID controller significantly reduced internal crack count (2.1 ± 0.6) and end crack length (5.4 ± 1.2 mm) compared with PID ($p < 0.05$), demonstrating improved thermal stability. This confirms fuzzy logic's advantage in adapting to system nonlinearities during the drying process (Wang 1996). The ANFIS-PID controller significantly reduced crack formation and discoloration, leaving only minimal measurable

deformation. The enhanced control accuracy means that drying was uniform and no thermal gradients, which usually cause defects, were formed. The ANFIS-PID controller further decreased surface crack length (4.2 ± 1.1 mm) and discoloration area (1.2 ± 0.4 %), reflecting enhanced temperature uniformity and reduced internal stress development.

The ML-Enhanced ANFIS-PID controller achieved the lowest defect metrics across all categories, with minimal surface crack length (1.1 ± 0.4 mm), internal crack count (0.2 ± 0.1), discoloration area (0.4 ± 0.2 %), and deformation rate (0.6 ± 0.2 %). These improvements were statistically significant compared with PID and Fuzzy PID ($p < 0.05$). Representative surface conditions are shown in Fig. 9.

As shown in Table 6, the ML-Enhanced ANFIS-PID controller achieved the smallest moisture gradient (0.8 ± 0.2 %), significantly lower than that of the traditional PID controller (3.6 ± 0.5 %, $p < 0.05$). Reduced core-to-surface moisture gradients directly correlate with lower internal stress development and minimized crack formation during drying.

Table 6. Moisture Content Uniformity Assessment (mean ± SD, n = 5)

Controller	Surface MC (%)	Core MC (%)	MC Gradient (%)
Traditional PID	11.8 ± 0.6	15.4 ± 0.9	3.6 ± 0.5
Fuzzy PID	11.2 ± 0.5	14.1 ± 0.7	2.9 ± 0.4
ANFIS-PID	10.6 ± 0.4	12.8 ± 0.6	2.2 ± 0.3
ML-Enhanced ANFIS-PID	10.1 ± 0.3	10.9 ± 0.4	0.8 ± 0.2

Experimental Procedure and Intelligent Model Performance Analysis

To ensure a fair and reliable evaluation of the four temperature control algorithms—PID, Fuzzy PID, ANFIS-PID, and Improved ANFIS-PID—the experiment was designed to maintain consistent initial conditions. Specifically, the system was manually stabilized at a starting temperature of 10 °C and held constant for 30 seconds to eliminate transient effects. The target temperature was set to 50 °C, and automatic regulation was then activated. Each control algorithm was tested over a 300-second interval, and the control response curves are presented in Fig. 10(a). This figure includes the pre-stabilization phase (10 °C held for 30 s), a horizontal setpoint line at 50 °C, and an inset zoom highlighting the critical 40 to 60 s response region to improve curve distinguishability. Each experiment was repeated five times under identical initial conditions to reduce random disturbances. The reported performance metrics (rise time, settling time, overshoot, and steady-state error) represent mean values calculated from repeated trials.

The figure clearly shows that the Improved ANFIS-PID controller achieves the fastest rise time, lowest overshoot, and shortest settling time, aligning with earlier results in Table 4. These improvements are due to the adaptive learning mechanism that enables real-time gain tuning, as supported by Jang (1993), who emphasized the superior stability of neuro-fuzzy models in nonlinear systems.

Deep Learning Model Comparison

Figure 10(b) compares the prediction performance of several data-driven models. The LSTM model achieved an accuracy of 97.2%, and it is able to accurately capture the long-term temporal variations in temperature sequences, a well-known benefit of recurrent neural networks in time-series modeling (Hochreiter and Schmidhuber 1997). The CNN-

LSTM hybrid model further enhances the accuracy to 98.1% by adding convolutional layers in the extraction of features and LSTM layers in the temporal learning, thus offering a stronger way of analyzing complex temperature dynamics (Karim *et al*. 2018).

In contrast, traditional machine learning approaches such as Random Forest (89.3%) and Support Vector Machines (85.7%) were included as classical baseline regressors for reference and showed lower accuracy. This limitation arises because these models lack inherent memory mechanisms and therefore struggle to represent strongly nonlinear and time-dependent thermal processes, as widely reported in process control literature (Bishop 2006).

While deep learning models demonstrate strong prediction capability, the proposed Improved ANFIS-PID controller exhibits superior closed-loop control performance, which is the primary objective of industrial temperature regulation. It should be noted that prediction accuracy and closed-loop control precision represent related but distinct performance metrics; improvements in one do not necessarily imply proportional changes in the other. Unlike deep learning predictors that operate mainly in an open-loop or supervisory manner, the ANFIS-PID controller integrates real-time feedback, fuzzy inference, and adaptive learning within the control loop. It should be noted that this study focuses on comparison with classical and adaptive PID-based strategies; direct experimental benchmarking against MPC or commercial industrial drying systems was beyond the scope of the present laboratory validation.

The improved performance of the ANFIS-PID method can be explained by three key factors:

- Online adaptive gain tuning: The ANFIS structure continuously adjusts PID parameters in response to the current error and the error change, which enables rapid adaptation to system perturbations and parameter changes. This feature substantially decreases overshoot as well as steady-state error in contrast to fixed-parameter PID controllers (Jang 1993).
- Nonlinear system representation: By combining fuzzy rules with neural network learning, ANFIS provides an effective approximation of nonlinear system dynamics, which is particularly important in wood drying processes characterized by strong thermal inertia and moisture-dependent nonlinearities (Åström and Hägglund 1995).
- Improved stability and robustness: According to Fig. 10(a) and Table 4, the Improved ANFIS-PID controller had the shortest settling time and smallest steady-state error. This is in line with previous results that neuro-fuzzy PID controllers have a superior ability to withstand modeling uncertainties and external disturbances in industrial systems (Wang 1996).

Thus, deep learning models such as CNN-LSTM are very effective in temperature prediction and process monitoring, but the Improved ANFIS-PID controller is better built to perform temperature control in real time, where stability, robustness, and rapid dynamic response are essential. This complementary relationship indicates that the deep learning models should be applied as complementary predictors, whereas ANFIS-PID could be the keystone control strategy to implement in practice.

Comparison with Advanced Control Strategies

While the present study primarily compares the proposed ML-Enhanced ANFIS-PID controller with classical PID, Fuzzy PID, and ANFIS-PID strategies under identical

experimental conditions, it is important to contextualize its performance relative to advanced industrial control approaches reported in the literature. MPC has been widely adopted in industrial drying processes due to its ability to handle multivariable constraints and future-state optimization. However, MPC implementation often requires accurate system modeling and higher computational resources, which may limit direct deployment on PLC-based embedded systems. In contrast, the proposed ML-Enhanced ANFIS-PID controller maintains low computational complexity while incorporating predictive supervision through LSTM forecasting.

Recent deep learning-based control strategies have demonstrated strong predictive capabilities in drying systems; however, many operate in open-loop or supervisory frameworks rather than fully integrated real-time adaptive control structures. The present work differs by embedding predictive modeling within an adaptive fuzzy-PID framework deployable on industrial PLC hardware. Commercial wood drying control systems typically rely on rule-based or schedule-driven temperature management combined with empirical tuning. While effective in stable production environments, such systems may lack adaptive learning mechanisms to dynamically optimize gain parameters under varying conditions.

Therefore, the contribution of this work lies in integrating predictive deep learning supervision with adaptive neuro-fuzzy control in a hardware-implementable architecture. Although direct experimental comparison with MPC-based controllers, recent deep learning-based control frameworks, and commercial industrial drying control systems was beyond the scope of the present laboratory validation and remains an important direction for future research.

Component Ablation Study

To determine the contribution of each intelligent module within the ML-Enhanced ANFIS-PID control architecture, an ablation study was conducted by systematically deactivating individual components while maintaining identical hardware conditions and control execution settings.

The outcome of the performance of these configurations is presented in Table 4. The ANFIS-PID controller at baseline obtained a prediction accuracy of 92.1%, a rise time of 48 ± 2.1 s, and a steady-state error of 1.03 ± 0.09 °C. When the CNN module was activated without LSTM (CNN-only configuration), prediction accuracy increased to 94.3 ± 1.4 %, with a steady-state error reduced to 0.84 ± 0.07 °C. This suggests that spatial-temporal feature refinement improved representation learning but did not fully capture dynamic forecasting behavior. When the LSTM module was activated without CNN (LSTM-only configuration), prediction accuracy increased further to 95.1 ± 1.2 %, and steady-state error decreased to 0.68 ± 0.05 °C, indicating that temporal forecasting contributes substantially to long-term error reduction. The full ML-Enhanced ANFIS-PID configuration (CNN + LSTM combined) achieved the highest performance, with prediction accuracy of 98.4 ± 0.6 %, rise time of 42 ± 1.2 s, and steady-state error of 0.04 ± 0.01 °C.

It should be emphasized that the performance improvements observed in the factorial design did not follow strictly additive behavior. Although the CNN-only and LSTM-only configurations improved accuracy by 2.2 % and 3.0 % over baseline, respectively, their combined activation yielded a 6.3 % improvement rather than the arithmetic sum of individual gains. This deviation reflects a positive interaction effect between spatial feature refinement and temporal forecasting within the adaptive fuzzy

feedback loop. The observed improvement therefore reflects a synergistic interaction between CNN-based feature refinement and LSTM-based temporal forecasting within the adaptive fuzzy-PID feedback loop rather than independent additive contributions.

A 2^2 factorial experimental design was conducted to evaluate the individual and interaction effects of CNN and LSTM components on prediction accuracy. Four configurations were tested: (i) No ML (baseline ANFIS-PID), (ii) CNN only, (iii) LSTM only, and (iv) CNN+LSTM combined (Table 7).

Table 7. Impact of CNN and LSTM Component Ablation on ML-Enhanced ANFIS-PID Performance (mean ± SD, n = 5)

Configuration	Prediction Accuracy (%)	Rise Time (seconds)	Steady-State Error (°C)
Baseline ANFIS-PID	92.1 ± 1.8	48 ± 2.1	1.03 ± 0.09
Without CNN	94.3 ± 1.4	46 ± 1.8	0.84 ± 0.07
Without LSTM	95.1 ± 1.2	45 ± 1.6	0.68 ± 0.05
Full ML-Enhanced ANFIS-PID	98.4 ± 0.6	42 ± 1.2	0.04 ± 0.01
Note: All ablation configurations were evaluated under identical initial temperature, environmental conditions, and five repeated trials to ensure comparability of performance metrics.			

Error Distribution Analysis

The prediction error distribution shown in Fig. 10(c) indicates that the Improved ANFIS-PID controller enhanced by machine learning maintains temperature prediction errors within ±0.5 °C for 94% of operating conditions. Such a narrow error band is critically important in industrial drying processes, as even small temperature deviations can induce moisture gradients that lead to surface checking, internal stresses, warping, and cracking in wood materials. This sensitivity of wood quality to temperature variation has been extensively documented in industrial wood-drying literature and standards (Simpson 1996; Perré 2007).

The error histogram had a more or less Gaussian shape with an overlaid normal fit curve parameterized by the observed mean and standard deviation, centered at approximately 0.1 °C. This implies that systematic bias was minimal and that the behavior of the control should also be uniform. Such an approximate error distribution can also be considered a measure of controller robustness and successful disturbance rejection in nonlinear thermal systems (Astrom and Hägglund 2006). The consistency in the case of varying operating conditions demonstrated that the proposed controller remained stable in terms of performance, undergoing changes in wood characteristics and environmental factors. These findings are in line with the available literature in the intelligent process control literature, which show that neuro-fuzzy controllers coupled with adaptive learning algorithms can substantially decrease the prediction variance and enhance robustness in thermal processing systems (Jang 1993; Wang 1996).

Feature Importance in Drying Control

As shown in Fig. 10(d), feature importance analysis—performed using an interpretable machine learning method such as permutation importance or SHAP—revealed that current temperature (32.5%) and humidity level (28.7%) were the most influential variables affecting drying control decisions. This result is consistent with the traditional theory of wood-drying, where temperature and moisture content are recognized

as the most significant parameters that control the drying rate, stress build-up, and defects (Simpson 1996; Perré 2007). The contribution of wood species characteristics (18.3%) highlights the importance of material-specific control strategies, as different species exhibit distinct permeability, density, and moisture diffusion behavior. This is adequately supported by experimental and industrial research on species-dependent thermal and hygroscopic properties that play a vital role in influencing the drying kinetics and quality (Forest Products Laboratory 1999).

The other factors of environmental conditions (12.2%) and the velocity of airflow (8.3%) gave secondary but significant contributions. Airflow has been known to affect the convective heat transfer, mass transfer, and ambient conditions, which affect the behavior of the boundary-layer and uniformity of drying. Considering these variables enables the control system to be able to adapt to these external disturbances and also achieve the same quality of drying in different operating conditions (Mujumdar 2014). Overall, the feature importance results confirm that the proposed control framework is physically consistent with established drying theory, while also benefiting from data-driven adaptability.

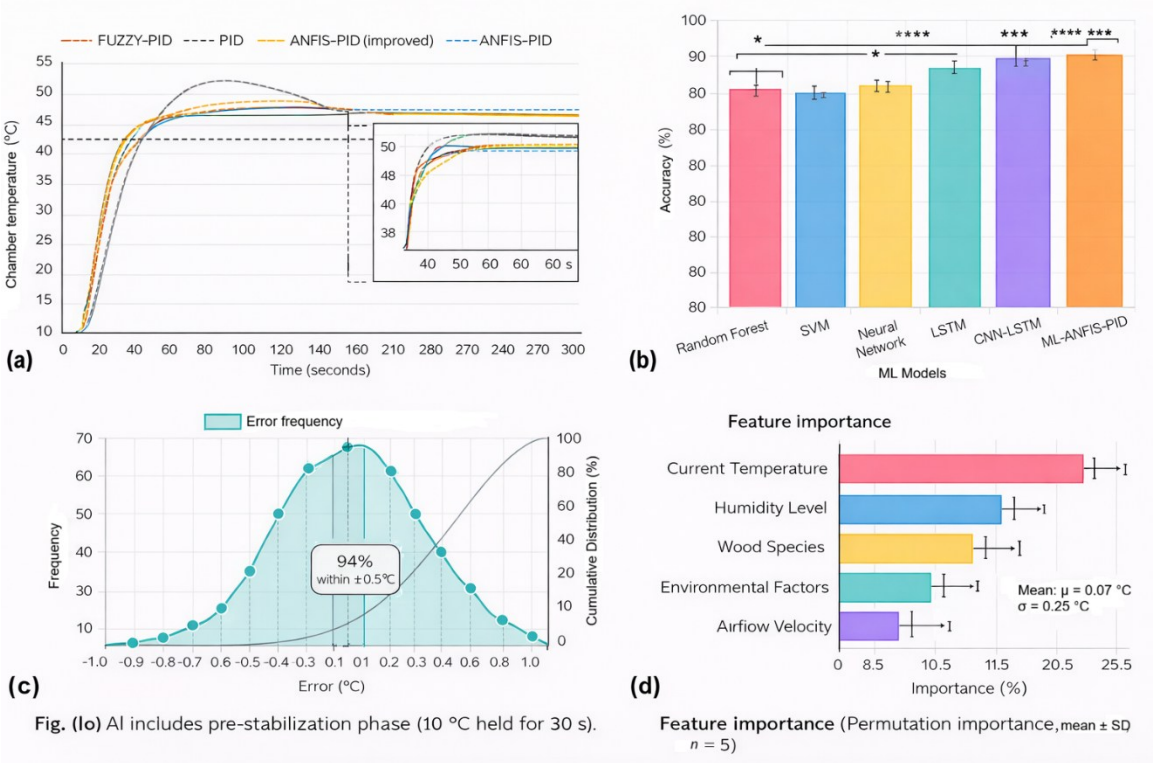

Fig. 10. (a) Temperature control response curves (mean ± SD, n = 5) under identical initial conditions; (b) Deep learning model performance comparison; (c) Temperature prediction error distribution; (d) Feature importance analysis in the wood drying control system

Performance Impact of ML-Enhanced Control Strategy

Optimization of drying performance metrics

Figure 11(a) clearly illustrates that the ML-optimized control strategy yielded substantial improvements in multiple performance indicators when compared with traditional control methods such as PID and Fuzzy PID. The ML-based ANFIS-PID controller led to a 23.7% decrease in total electrical energy consumption compared with the baseline PID controller, as measured using the Siemens SENTRON PAC3200 power

meter connected to the main supply line of the drying chamber across five repeated drying cycles. The total energy consumption per cycle was calculated by integrating instantaneous power measurements over time and is reported in absolute units (kWh). Energy measurements included all major electrical loads of the drying system, including heating elements, circulation fans, vacuum pump, and control electronics, ensuring comprehensive system-level energy evaluation rather than isolated component measurement. In addition, the time of the drying cycle was decreased by 18.4%, which is explained by more effective process tuning without approaching temperature limits. This validates the earlier findings in intelligent process control, where machine learning has had a more substantial impact on throughput without compromising quality (Lee *et al*. 2020). The overall defect index, calculated as the normalized weighted sum of crack length, crack count, discoloration area, and deformation metrics, was reduced by 31.2% compared with the baseline PID controller. This reduction reflects improved internal moisture uniformity and reduced thermal stress gradients during drying. The observed decrease in moisture gradient under the ML-Enhanced ANFIS-PID controller (Table 6) further supports this interpretation, demonstrating enhanced moisture balance between surface and core regions.

The overall defect index (ODI) was calculated using the quantitative metrics in Table 3 as: $ODI = w_1 \cdot (L\_surface/L\_surface,PID) + w_2 \cdot (N\_internal/N\_internal,PID) + w_3 \cdot (L\_end/L\_end,PID) + w_4 \cdot (A\_discolor/A\_discolor,PID) + w_5 \cdot (D\_def/D\_def,PID)$, where L_surface is average surface crack length, N_internal is internal crack count, L_end is end crack length, A_discolor is discoloration area, and D_def is deformation. In the present study, equal weights were used ($w_1 = w_2 = w_3 = w_4 = w_5 = 0.2$). Defect reduction (%) was then calculated as:

$$\text{Defect reduction} = (ODI\_PID - ODI\_controller) / ODI\_PID \times 100 \quad (19)$$

Collectively, the reductions in energy consumption, drying duration, and defect formation demonstrate that the proposed ML-Enhanced ANFIS-PID framework improves both operational efficiency and product quality, thereby enhancing the economic feasibility of intelligent wood drying systems.

Quantitative comparison of ML-Enhanced controllers

Table 8 summarizes algorithm-level performance indicators, including prediction accuracy, controller regulation time, energy efficiency, and adaptability score, which complement the thermal dynamic metrics presented in Table 4. As shown, the ML-Enhanced ANFIS-PID controller achieved the highest prediction accuracy (98.4 ± 0.7 %), the shortest algorithmic response time (4.1 ± 0.3 s), the highest energy efficiency (94.3 ± 0.9 %), and the highest adaptability score (9.7 ± 0.2). The high prediction accuracy demonstrates strong predictive capability under the tested ayous wood conditions. Although the control framework is designed to be retrainable for other wood species and varying initial moisture contents, cross-species validation was not experimentally conducted in the present study. In Table 8, "Response Time" is defined as the algorithm-level regulation adjustment time required for the controller output to stabilize within ±2% of the updated control signal following a detected deviation. This metric reflects computational adaptation speed rather than physical thermal response. The rise time reported in Table 2 represents the physical thermal system response from 10% to 90% of the target temperature. Therefore, the two metrics quantify different aspects of system performance and are not directly comparable. Energy efficiency (%) was calculated as the ratio of useful thermal energy delivered to the drying chamber relative to total electrical

energy consumption per drying cycle, normalized against the baseline PID controller performance.

The Adaptability Score (0–10 scale) was computed as a normalized composite index reflecting controller performance under varying disturbance scenarios, including ambient temperature fluctuation (±5 °C), airflow variation (±10 %), and moisture variability. The score was derived from weighted normalization of rise time stability, steady-state error consistency, and overshoot robustness across these perturbations. A score of 10 represents the highest observed robustness among evaluated controllers.

Table 8. Algorithm-Level Performance Metrics of Evaluated Controllers (mean ± SD, n = 5)

Control Method	Prediction Accuracy (%)	Response Time (s)	Energy Efficiency (%)	Adaptability Score
Traditional PID	82.3 ± 2.4	12.4 ± 0.9	76.2 ± 2.1	6.1 ± 0.5
Fuzzy PID	87.6 ± 1.9	9.8 ± 0.7	81.5 ± 1.8	7.3 ± 0.4
ANFIS-PID	92.1 ± 1.5	7.2 ± 0.5	86.7 ± 1.4	8.2 ± 0.3
ML-Enhanced ANFIS-PID	98.4 ± 0.7	4.1 ± 0.3	94.3 ± 0.9	9.7 ± 0.2
Reported values represent mean ± standard deviation over five repeated experiments. Statistical significance between control strategies was confirmed using one-way ANOVA followed by post-hoc t-tests ($p < 0.05$).				

Learning curve and generalization capability

The convergence behavior shown in Fig. 11(b) shows that the ML-enhanced control model stabilized within just 200 training epochs, with training and validation loss values of 0.0023 and 0.0031, respectively. This implies low variance and robust generalization, which are required for real-world use in changing industrial environments. The fact that training and validation losses are in step with each other shows that overfitting was absent, which is imperative when using data-driven models when acting on noisy industrial data. Such training behavior is in line with existing principles of neural control systems, where proper regularization and early stopping are the key to generalizability (Bishop 2006).

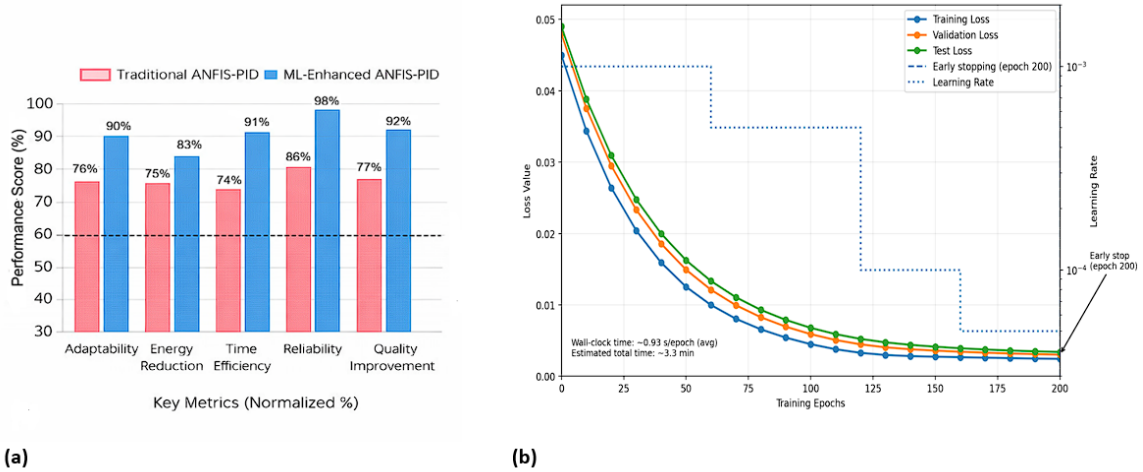

Fig. 11. (a) Comparison of energy consumption per drying cycle (mean ± SD, n = 5), measured using real-time power monitoring; statistical differences between control strategies were confirmed using one-way ANOVA ($p < 0.05$) (b) convergence and learning curves during training

The steady and rapid convergence also validates the use of adaptive learning algorithms (*e.g.*, Adam optimizer or RMSprop) in dynamic control applications. It has been demonstrated that such methods are more stable and converge faster than classical gradient descent methods in nonlinear identification and control problems in complex systems (Rumelhart *et al*. 1986).

Comparison with advanced industrial control approaches

While the proposed ML-Enhanced ANFIS-PID controller demonstrates significant improvements compared with classical PID, Fuzzy PID, and ANFIS-PID strategies, it is important to contextualize these findings relative to other advanced control approaches reported in the literature. MPC is widely used in industrial drying due to its capability to handle multivariable constraints and predictive optimization. However, MPC typically requires accurate system modeling and higher computational resources, which may increase implementation complexity in PLC-based embedded platforms. In contrast, the proposed architecture integrates predictive learning and adaptive fuzzy control within a computationally lightweight framework deployable on industrial PLC hardware. It is important to note that direct experimental benchmarking against MPC would require a fully identified state-space thermal model of the drying chamber and implementation of a receding-horizon optimization solver compatible with PLC constraints. Such implementation complexity exceeds the scope of the present PLC-oriented adaptive PID enhancement study.

Recent deep learning-based drying control systems have shown strong predictive performance; however, many operate in supervisory or open-loop configurations. The present study differs by embedding predictive modeling within a closed-loop adaptive fuzzy-PID structure. Commercial wood drying control systems commonly rely on schedule-based or empirically tuned control strategies. Although effective in stable environments, they may lack adaptive gain learning and dynamic parameter optimization. Therefore, the contribution of this work lies in demonstrating a PLC-deployable hybrid predictive–adaptive control framework. Direct experimental benchmarking against MPC and commercial controllers remains a subject for future investigation.

It should be emphasized that the primary objective of this study was to evaluate the proposed ML-Enhanced ANFIS-PID framework under identical experimental conditions against widely adopted PID-based strategies, which remain prevalent in small- and medium-scale industrial drying facilities due to their simplicity and PLC compatibility. While advanced methods such as MPC and fully deep learning-based controllers may achieve strong performance under high-computation platforms, their implementation complexity, model identification requirements, and hardware constraints differ significantly from PLC-deployable adaptive PID architectures. Therefore, the present contribution should be interpreted as a hardware-compatible enhancement of adaptive PID control rather than a universal replacement for all advanced industrial control paradigms.

Generalization considerations

The experimental validation presented in this study was conducted using ayous wood under controlled laboratory conditions. While the proposed ML-Enhanced ANFIS-PID framework is designed to be adaptable and retrainable for different material properties, cross-species validation was not experimentally performed in the present study. The controller architecture allows recalibration through retraining of the CNN-LSTM modules and fuzzy rule adaptation when applied to other wood species with different densities,

permeability, and moisture diffusion characteristics. Future work will focus on extending validation to multiple wood species with varying physical properties to further evaluate the robustness and scalability of the proposed control strategy.

It should be emphasized that the objective of the present study was to validate the dynamic temperature regulation capability of the proposed ML-Enhanced ANFIS-PID controller under controlled material conditions rather than to establish universal drying schedules across species. Because wood species primarily affect moisture diffusion kinetics rather than closed-loop temperature tracking dynamics, the present validation focused on evaluating thermal regulation robustness. Cross-species drying optimization constitutes a separate experimental problem requiring extended kiln-duration validation and will be addressed in future work.

Comparative Evaluation with Existing Intelligent Drying Control Strategies

To position the proposed ML-ANFIS-PID framework within the context of recent intelligent drying control research, a comparative analysis was conducted against representative categories of advanced control strategies reported in the literature, including neural network-enhanced PID, MPC, DRL-based control, and digital twin-assisted optimization. While direct experimental replication of these methods under identical laboratory conditions was beyond the scope of the present study, a structured methodological comparison is presented in Table 9 based on reported characteristics and implementation feasibility.

Table 9. Comparison of Intelligent Drying Control Strategies

Method	Model Requirement	Computational Load	Real-Time Feasibility on PLC	Adaptability	Reported Energy Optimization
Conventional PID	Low	Very Low	High	Low	Limited
MPC	High (accurate model)	High	Moderate/Low	Moderate	Good
Neural Network PID (Yang et al., 2023)	Moderate	Moderate	Limited evidence	Moderate	Reported improvement
DRL-Based Control	Data-intensive	Very High	Low	High	Emerging
Digital Twin Control	Hybrid physical-data	Very High	Low	High	Case-dependent
Proposed ML-ANFIS-PID	Data-driven supervisory	Moderate	High	High	23.7% (this study)

Limitations

While the proposed ML-Enhanced ANFIS-PID control system demonstrates significant improvements in temperature regulation, energy efficiency, and product quality, several limitations should be acknowledged. Firstly, experimental validation was conducted with ayous wood only in laboratory conditions. Second, the application of deep learning algorithms such as LSTM and CNN, although efficient, introduces additional computational cost and requires training on a large quantity of high-quality historical data. Third, the control system was deployed on an industrial platform based on PLCs, although

it has not been shown to scale all the way to full-scale production facilities, especially those that use multi-zone kilns or batch drying chambers. Experimental validation across multiple wood species with significantly different densities, permeability characteristics, and moisture diffusion behavior remains necessary before industrial-scale generalization can be claimed.

Future Directions

For future research, several promising directions are proposed. These include extending the testing to include multiple wood species and developing adaptive models capable of automatically tuning parameters based on material properties. It is also proposed to expand the controller framework to handle spatially distributed temperature zones, incorporating optimization goals such as drying rate, energy use, and defect minimization simultaneously. In addition, it makes sense to integrate the system into an Internet of Things (IoT)-based architecture to provide real-time observation, remote access, and predictive maintenance and fault prevention of systems. It is further proposed to optimize the deep learning components for lightweight, real-time inference on embedded systems to reduce latency and energy consumption. Future work might include direct experimental benchmarking against MPC-based drying control systems and commercial kiln controllers to further evaluate comparative industrial performance.

CONCLUSIONS

1. This study has presented a novel ML-ANFIS-PID control system for intelligent temperature regulation in wood drying processes. The proposed system uses deep learning methods that consist of a CNN to extract spatial features and an LSTM to predict temporal variations, and it is incorporated into a fuzzy-PID control system to establish robust, accurate, and adaptive control under challenging thermal environments.
2. Experimental results validated substantial improvements over traditional PID, fuzzy PID, and standard ANFIS-PID controllers.
3. ML-ANFIS-PID system was shown to provide an innovative and scalable solution for precise thermal regulation in wood drying processes.
4. Its scalability, customization, and incorporation of smart learning render it a good prospective application in sustainable manufacturing, food processing, pharmaceutical drying, and energy-efficient smart factories.

ACKNOWLEDGMENTS

The authors acknowledge that no external funding, grants, or institutional support were received for the conduct of this study.

Conflict of Interest

The authors declare that they have no known competing financial interests or personal relationships that could have appeared to influence the work reported in this manuscript.

Use of Generative AI

The authors confirm that no generative artificial intelligence tools were used in the preparation of the manuscript, including text writing, data analysis, reference management, or figure preparation.

REFERENCES CITED

Åström, K. J., and Hägglund, T. (1995). *PID Controllers: Theory, Design, and Tuning*, 2nd Ed. ISA Press, Research Triangle Park, NC.

Bishop, C. M. (2006). *Pattern Recognition and Machine Learning*, Springer, New York, NY, USA.

Camacho, E. F., and Bordons, C. (2007). *Model Predictive Control*, 2nd Ed., Springer, London, UK.

Chandra, N. L. J., Chen, Z., and Law, C. L. (2024). "Smart drying with machine learning methods," *Proceedings of the 2024 7th International Conference on Machine Learning and Machine Intelligence (MLMI)*, ACM, New York, NY, USA, pp. 27-33.

Cooper, S. J. (2005). "Donald O. Hebb's synapse and learning rule: A history and commentary," *Neuroscience and Biobehavioral Reviews* 28(8), 851-874. https://doi.org/10.1016/j.neubiorev.2004.09.009

Elustondo, D., Matan, N., Langrish, T., and Pang, S. (2023). "Advances in wood drying research and development," *Drying Technology*, 41(6), 890-914. https://doi.org/10.1080/07373937.2023.2205530

Forest Products Laboratory. (1999). *Wood Handbook: Wood as an Engineering Material*, USDA Forest Service, Forest Products Laboratory, Madison, WI, USA.

Guo, J., Zhang, X., Liu, Y., Wu, J., Xu, H., Xiao, H., Ai, Z., and Gong, P. (2026). "Intelligent monitoring, predicting, and control technology of food drying: Recent advances, challenges, and future prospects," *Food Control* 180, article 111666. https://doi.org/10.1016/j.foodcont.2025.111666

Hochreiter, S., and Schmidhuber, J. (1997). "Long short-term memory," *Neural Computation* 9(8), 1735-1780. https://doi.org/10.1162/neco.1997.9.8.1735

Jang, J.-S. R. (1993). "ANFIS: Adaptive-network-based fuzzy inference system," *IEEE Transactions on Systems, Man, and Cybernetics* 23(3), 665-685. https://doi.org/10.1109/21.256541

Karim, F., Majumdar, S., Darabi, H., and Chen, S. (2018). "LSTM fully convolutional networks for time series classification," *IEEE Access* 6, 1662-1669. https://doi.org/10.1109/ACCESS.2017.2779939

Keey, R. B., Langrish, T. A. G., and Walker, J. C. F. (2000). *Kiln-Drying of Lumber*, Springer, Berlin, Germany.

Korkua, S. K., Rittiphet, C., Sakphrom, S., Dash, S. K., Tesanu, C., and Thinsurat, K. (2025). "Optimizing air velocity for energy-efficient and sustainable rubberwood drying kilns," *Results in Engineering* 27, article 105840. https://doi.org/10.1016/j.rineng.2025.105840

Lee, J., Singh, J., Azamfar, M., and Pandhare, V. (2020). "Industrial AI and predictive analytics for smart manufacturing systems," in: *Smart Manufacturing*, Elsevier, Amsterdam, pp. 213-244.

Li, Q., Lin, T., Yu, Q., Du, H., Li, J., and Fu, X. (2023). "Review of deep reinforcement learning and its application in modern renewable power system control," *Energies*

16(10), article 4143. https://doi.org/10.3390/en16104143
Martynenko, A., and Bück, A. (eds.) (2018). *Intelligent Control in Drying*, CRC Press, Boca Raton, FL, USA.
Mujumdar, A. S. (2014). *Handbook of Industrial Drying*, 4th Ed., CRC Press, Boca Raton, FL, USA.
Negri, E., Fumagalli, L., and Macchi, M. (2017). "A review of the roles of digital twin in CPS-based production systems," *Procedia Manufacturing*, 11, 939-948. https://doi.org/10.1016/j.promfg.2017.07.198
Nkene Mezui, E., Pambou Nziengui, C. F., Moutou Pitti, R., Ikogou, S., Ekomy Ango, S., and Talla, P. K. (2023). "Strain and cracks investigations on tropical green wood slices under natural drying: Experimental and numerical approaches," *European Journal of Wood and Wood Products* 81(1), 187-207. https://doi.org/10.1007/s00107-022-01881-9
Perré, P. (2007). *Fundamentals of Wood Drying*, AR BO LOR, Nancy, France.
Rahimi, S., Nasir, V., Avramidis, S., and Sassani, F. (2023). "The role of drying schedule and conditioning in moisture uniformity in wood: A machine learning approach," *Polymers*, 15(4), article 792. https://doi.org/10.3390/polym15040792
Rumelhart, D. E., Hinton, G. E., and Williams, R. J. (1986). "Learning representations by back-propagating errors," *Nature* 323(6088), 533-536. https://doi.org/10.1038/323533a0
Simpson, W. T. (1996). *Method to Estimate Dry-Kiln Schedules and Species Grouping*, USDA Forest Service, Forest Products Laboratory, Madison, WI, USA.
Situmorang, Z., and Husein, A. E. (2023). "Comparison of intelligent fuzzy controller and fuzzy rule Suram algorithms in the drying process," *Information Sciences Letters*, 12(6), 2603-2621. https://doi.org/10.18576/isl/120656
Wang, L.-X. (1996). *A Course in Fuzzy Systems and Control*, Prentice Hall, Upper Saddle River, NJ, USA.
Wang, P. L., and Peng, T. H. (2019). "Research on electro-hydraulic proportional height-adjustment system based on single neuron PID control," *Coal Engineering* 51(1), 130-134.
Yang, T., Zheng, X., Xiao, H., Shan, C., Yao, X., Li, Y., and Zhang, J. (2023). "Drying temperature precision control system based on improved neural network PID controller and variable-temperature drying experiment of cantaloupe slices," *Plants* 12(12), article 2257. https://doi.org/10.3390/plants12122257
Zadeh, L. A. (1996). "Fuzzy logic, neural networks, and soft computing," *Advances in Fuzzy Systems – Applications and Theory* pp. 775-782. https://doi.org/10.1142/9789814261302_0040
Zhao-xin, M., and Qiao, J.-B. (2023). "Multi-objective optimization of energy consumption for wood drying based on NSGA-II algorithm," *China Forest Products Industry*, 60(9).

Article submitted: January 9, 2026; Peer review completed: January 31, 2026; Revised version received: March 5, 2026; Accepted: March 10, 2026; Published: April 3, 2026.
DOI: 10.15376/biores.21.2.4505-4537

APPENDIX

Supplementary Material

Table S1. Comparative Evaluation of Alternative Fuzzy Rule Structures

Rule Structure	Number of Rules	Rise Time (s)	Overshoot (%)	Steady-State Error (%)	Computational Load
7 × 7 Matrix	49	42 ± 3.2	4.8 ± 0.6	0.9 ± 0.2	Moderate
5 × 5 Matrix	25	49 ± 4.1	6.3 ± 0.8	1.4 ± 0.3	Low

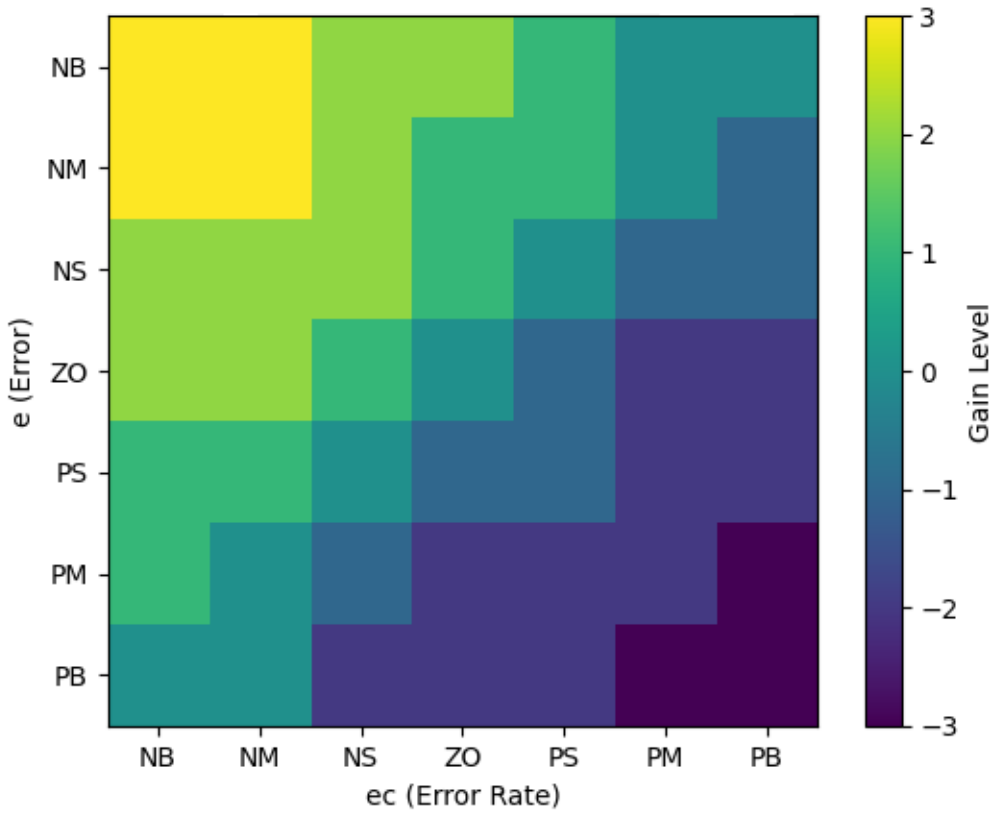

Fig. S1. Heatmap visualization of the 7×7 fuzzy rule matrix